AD-A189 133 FUNDAMENTAL STUDIES IN THE MOLECULAR BASIS OF LASER INDUCED RETINAL DAMAGE(U) CORNELL UNIV ITHACA NY SCHOOL OF APPLIED AND ENGINEERING PHYSICS A LEWIS SEP 84 1/1

UNCLASSIFIED DAMD17-79-C-9041 F/G 6/18 NL

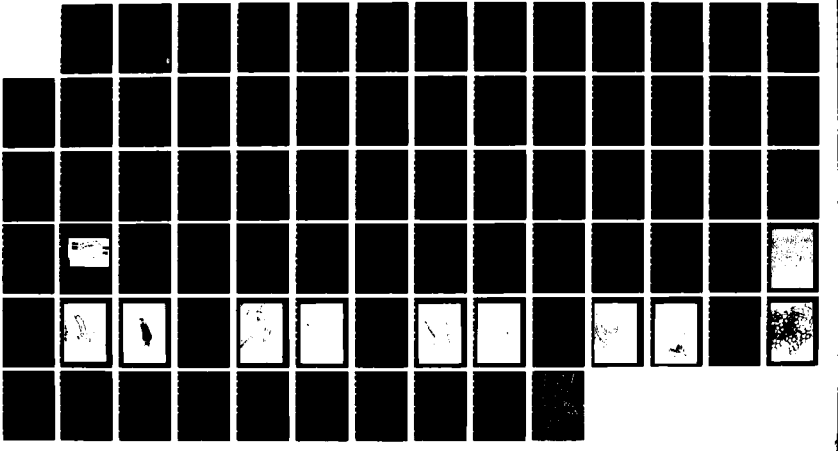

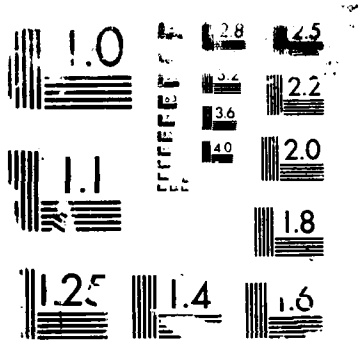
1.0
1.1
1.25
1.4
1.6
1.8
2.0
2.2
2.5
2.8
3.2
3.6
4.0

AD _____

FUNDAMENTAL STUDIES IN THE MOLECULAR BASIS OF LASER INDUCED RETINAL DAMAGE

Annual Report

September 1984

Aaron Lewis, Ph.D.

Supported by

U.S. ARMY MEDICAL RESEARCH AND DEVELOPMENT COMMAND
Fort Detrick, Frederick, Maryland 21701-5012

Contract No. DAMD17-79-C-9041

Cornell University
School of Applied and Engineering Physics
Ithaca, New York 14853

SECURITY CLASSIFICATION OF THIS PAGE

REPORT DOCUMENTATION PAGE

Form Approved
OMB No 0704-0188
Exp Date Jun 30 1986

1a REPORT SECURITY CLASSIFICATION: Unclassified	1b RESTRICTIVE MARKINGS
2a SECURITY CLASSIFICATION AUTHORITY	3 DISTRIBUTION/AVAILABILITY OF REPORT: Approved for public release; distribution unlimited
2b DECLASSIFICATION/DOWNGRADING SCHEDULE	
4 PERFORMING ORGANIZATION REPORT NUMBER(S)	5 MONITORING ORGANIZATION REPORT NUMBER(S)
6a NAME OF PERFORMING ORGANIZATION: Cornell University / 6b OFFICE SYMBOL (If applicable)	7a NAME OF MONITORING ORGANIZATION
6c ADDRESS (City, State, and ZIP Code): School of Applied and Engineering Physics, Ithaca, New York 14853	7b ADDRESS (City, State, and ZIP Code)
8a NAME OF FUNDING/SPONSORING ORGANIZATION: U. S. Army Medical Research & Development Command / 8b OFFICE SYMBOL (If applicable)	9 PROCUREMENT INSTRUMENT IDENTIFICATION NUMBER: DAMD17-79-C-9041
8c ADDRESS (City, State, and ZIP Code): Fort Detrick, Frederick, Maryland 21701-5012	10 SOURCE OF FUNDING NUMBERS

PROGRAM ELEMENT NO.	PROJECT NO	TASK NO	WORK UNIT ACCESSION NO
62772A	3E162, 772A878	BA	210

11 TITLE (Include Security Classification)
(U) Fundamental Studies in the Molecular Basis of Laser Induced Retinal Damage

12 PERSONAL AUTHOR(S)
Aaron Lewis, Ph.D.

13a TYPE OF REPORT	13b TIME COVERED	14 DATE OF REPORT (Year, Month, Day)	15 PAGE COUNT
Annual Report	FROM 9/83 TO 8/84	1984 September	

16 SUPPLEMENTARY NOTATION

17 COSATI CODES			18 SUBJECT TERMS (Continue on reverse if necessary and identify by block number)
FIELD	GROUP	SUB-GROUP	
20	05		
06	18		

19 ABSTRACT (Continue on reverse if necessary and identify by block number)

20 DISTRIBUTION/AVAILABILITY OF ABSTRACT	21 ABSTRACT SECURITY CLASSIFICATION
☐ UNCLASSIFIED/UNLIMITED ☒ SAME AS RPT ☐ DTIC USERS	

22a NAME OF RESPONSIBLE INDIVIDUAL	22b TELEPHONE (Include Area Code)	22c OFFICE SYMBOL
Mrs. Judy Pawlus	301-663-7325	SGRD-RMI-S

DD FORM 1473, 84 MAR — 83 APR edition may be used until exhausted. All other editions are obsolete.

SECURITY CLASSIFICATION OF THIS PAGE

FOREWORD

Citations of commercial organizations and trade names in this report do not constitute an official Department of the Army endorsement or approval of the products or services of these organizations.

In conducting the research described in this report, the investigator(s) adhered to the "Guide for the Care and Use of Laboratory Animals," prepared by the Committee on Care and Use of Laboratory Animals of the Institute of Laboratory Animal Resources, National Research Council (DHEW Publication No. (NIH) 78-23, Revised 1978).

TABLE OF CONTENTS

General Overview

In this section we will describe the tremendous advances made in the past year and a half in our work for the Ocular Hazards Program at the Letterman Army Institute of Research (LAIR). Our research has seen the first application of femtosecond lasers to the visual system. This research is giving new insights into how these ultimate laser sources interact with biological tissue in general and with the visual system in particular. Also under our contract with LAIR we have discovered during this period that simple anions can activate visual photoreceptors in the dark. Among these anionic activators is the commonly used dental agent fluoride. The data on in vitro preparations indicate that these anions modulate photoreceptor biochemistry and may effect photoreceptors sensitivity. In addition, we have continued our research into identifying selectively and spatially the image of various elemets in photoreceptors and adjacent tissue. We were able to extend our preparation procedures to view the elemental compostion of such components as melanin granules. The sensitive and selective spatial images we are getting should play important roles in extending our understanding of the fundamental mechanisms of laser damage. We have also developed complementary techniques to view, in light microscopy, actin filaments in photoreceptors. The stain we use is simple, highly specific and could possibly be extended to living cells. Furthermore, these staining procedures we have developed can already be applied universally to study laser damaged retina. We have also continued to study the protective nature of oil droplets in the turtle. For these studies we have been able to design and to use a Raman microprobe to obtain single oil droplet spectra. Finally, over

the last few months we have obtained data demonstrating rapid mechanical motions in vertebrate photoreceptors. Such rapid mechanical motions which parallel electrophysiological responses in the cell may lie at the very basis of photoreceptor function. Laser damage mechanisms we believe should now be reevaluated in terms of this new data. The effect of laser light on these newly discovered mechanical motions will surely lead to new and improved understandings of low level laser ocular hazards.

In the next six sections we will describe these significant advances of the past year and a half. Figures will be numbered separately in each section from one but the references will be numbered consecutively throughout the proposal. There are many xerox copies of photographs distributed throughout this section. Since 18 copies of the proposal were required it was prohibitive to make so many copies of the photographs. Ms. Becky McHenry at LAIR has one full set on file.

I. The First Application of Femtosecnd Lasers in the Ocular Hazards Program

A. Introduction

With existing equipment and under our contract with the Letterman Army Institute of Research the tunable femtosecond laser system we specified in our last proposal has been assembled. The femtosecond system was built, as proposed, in year one of the contract. In this section we will describe both the system and the very exciting results we have obtained during the contract's second year. The instrument is now ready to be applied to the variety of problems being considered in the Division of Ocular Hazards at LAIR. In addition, we believe that new safety standards will have to define these unique and important new laser sources which are the ultimate, 10^{-15}S, timing devices and will surely have wide-ranging military applications.

B. The Femtosecond Laser System

The essence of the femtosecond laser system, which was built on the design of Fork et al (1), is a colliding-pulse, mode-locking (CPM) arrangement. A diagram of the device is seen in Fig. 1A. In this system a conventional CW argon ion laser is used at an output power of 3-7 W and an output wavelength of 514.5 nm together with a jet-stream dye laser with a rhodamine 6G active medium. The counterpropogating pulses interact in the saturable absorber, which is 3,3'-Diethyloxadicarbocyanine iodide, causing a transient grating tosynchronize and shorten the pulses.

To amplify the pulse, a three stage dye amplifier system labelled 1, 2, & 3 in Fig. 1B is pumped by a doubled Nd:Yag laser at 530 nm.

The femtosecond output of the CPM ring dye laser is fed into the amplifier stages at the point labelled pulse in. Each amplifier stage is separated by a saturable absorber that reduces amplifier temporal broadening. A grating pair compressor labelled 4 reduces group velocity broadening in the amplifier optics. Using this system, 1 mJ femtosecond pulses have been obtained at specific wavelengths.

To measure the time duration of the pulses we used a sum frequency generation scheme that we reported several years ago (2). In this scheme (see Figure 2A) the laser output is directed by mirror A onto a beam splitter B. Half of the beam intensity is reflected onto a stationary prism that returns the laser beam along the same optical path. The rest of the original beam intensity went through the beam splitter and impinged on a motor driven prism that also returned the beam along the same optical path. Both returning laser beams are then focused onto a $LiIO_3$ crystal and if and only if the two beams are coincident in time the sum frequency would be generated by the crystal and detected in the blue where photomultipliers are most sensitive. The result of this experiment is an autocorrelation of the pulse which is shown in Figure 2B to be 70 fsec.

C. Femtosecond Results

During the second year of the contract, as proposed, we obtained our first results on pigments of importance in the visual system. These, in fact, are the first data ever obtained with femtosecond spectroscopy on a biological system. Using two specific wavelengths available to us we were able to record the data seen in Figure 3. The energies available to us allowed us to study cone visual pgiments which absorb light in the red. Thus, since we wanted to move into studying

cone photoreceptors, we chose, as described in our last proposal, the mudpuppy as a good starting point because of the availability of material at a fairly reasonable price. In addition the mudpuppy cone visual pigment has been well studied at our available wavelengths of 570 nm and 620 nm (3). Using the pulses from the laser reduced in intensity to 10 μJ and focused to a diameter of 0.3 mm we found an increase in transmission (decrease in absorption) at 570 nm (see Figure 3). This represents a loss of ground state nolecules. The results at 570 nm are very accurate in terms of the time scales. The results at 620 nm, which represent a decrease in transmission, record the photochemical product being produced. However, because of index of refraction effects the time scale of these 620 nm results are not, in our present configuration, as accurate.

The 570 nm data already has presented us with a fascinating glimpse at the interaction of light with rhodopsins. Specifically, as you notice in the data, it takes two 80 fsec pulse before any change in transmission at 570 nm is detected. This is an amazing observation since it was thought that the interaction of light with matter is instantaneous. In fact all other "man-made" dyes studied by us do indeed have an instantaneous response to light as detected by the femtosecond laser system. Therefore, cone rhodopsins seem to have some unique mechanism that appears to protect the eye from responding to these very rapid pulses. This mechanism may be at the very basis of the energy capture and storage process in cone photreceptors.

In addition to this first investigation of the effect of such pulses in any biological system, we have repeated the above investigation with the photoreceptors in D_2O. The reason for this investigation

was to compare the kinetics of these primary processes in both H_2O, the natural solvent, and D_2O. Since we had previously demonstrated that photon capture and energy conversion is over in 1 psec in rhodopsin (4), the femtosecond system gave us the unique opportunity to investigate our earlier suggestion (5) that proton motion is stimulated by rhodopsin light-absorption. The results we got dramatically support out earlier suggestion (5). In D_2O (see Figure 4) both the excited state decay and the initial induction time before absorption are delayed probably by the slower movement of deuterons. Thus, we see, that the induction time, from time zero to the maximum transmission change at 570 nm, is 6 rather than the 3 pulses seen in the H_2O spectrum. Also, the decay of the rhodcpsin excited state monitored at 570 nm takes longer in D_2O. The dotted curve in the D_2O results is obtained at a power $>$ 10μJ. It appears that at these power levels non-linear phenomena are induced in the visual pigment. We deduce this from the power dependence of this high laser power spectrum.

Our data are demonstrating that we now have the tool to watch the very essence of these fundamental processes of light absorption and energy conversion in visual excitation. Our data also indicate that fsec pulses which are at the very limit of the time response of photochemical systems are inducing new phenomena in biological systems. Thus, we have to use and evaluate these pulses, at this ultimate of time resolution, not only from an ocular hazard standpoint but also from their effect on biological tissue in general. We plan to initiate this in the subsequent years of this contract with certain instrumental improvements.

Figure 1A Colliding Pulse Mode Laser Cavity Configuration

1B Femtosecond Pulse Amplifier

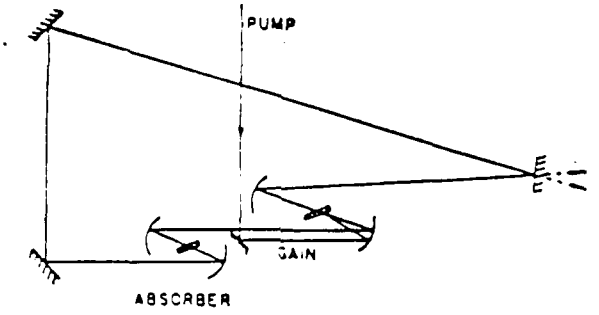

Figure 1A

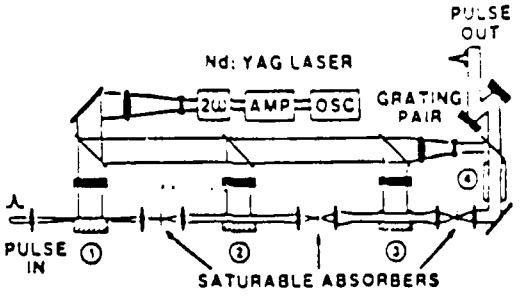

Figure 1B

Figure 2A Schematic Diagram of the Experimental Apparatus Used for Obtaining the Autocorrelation of Femtosecond Laser Pulses by the Sum Frequency of the Amplified Pulse.

2B Autocorrelation Function of the Amplified Pulse.

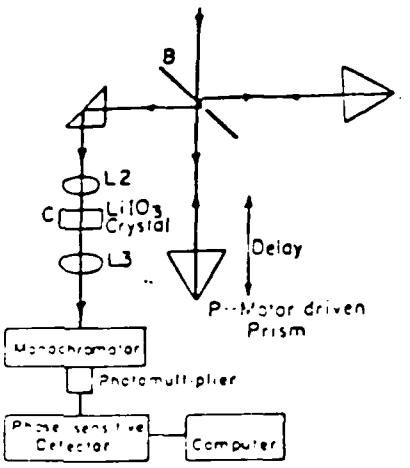

Figure 1A

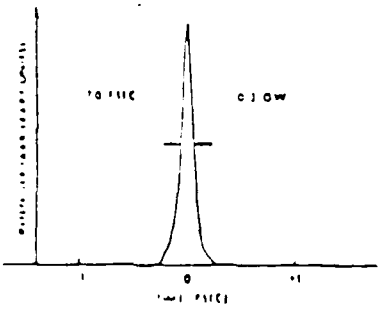

Figure 1B

Figure 3 Response of Cone Rhodopsin in H_2O to Femtosecond Excitation. Each point is 80 fsec.

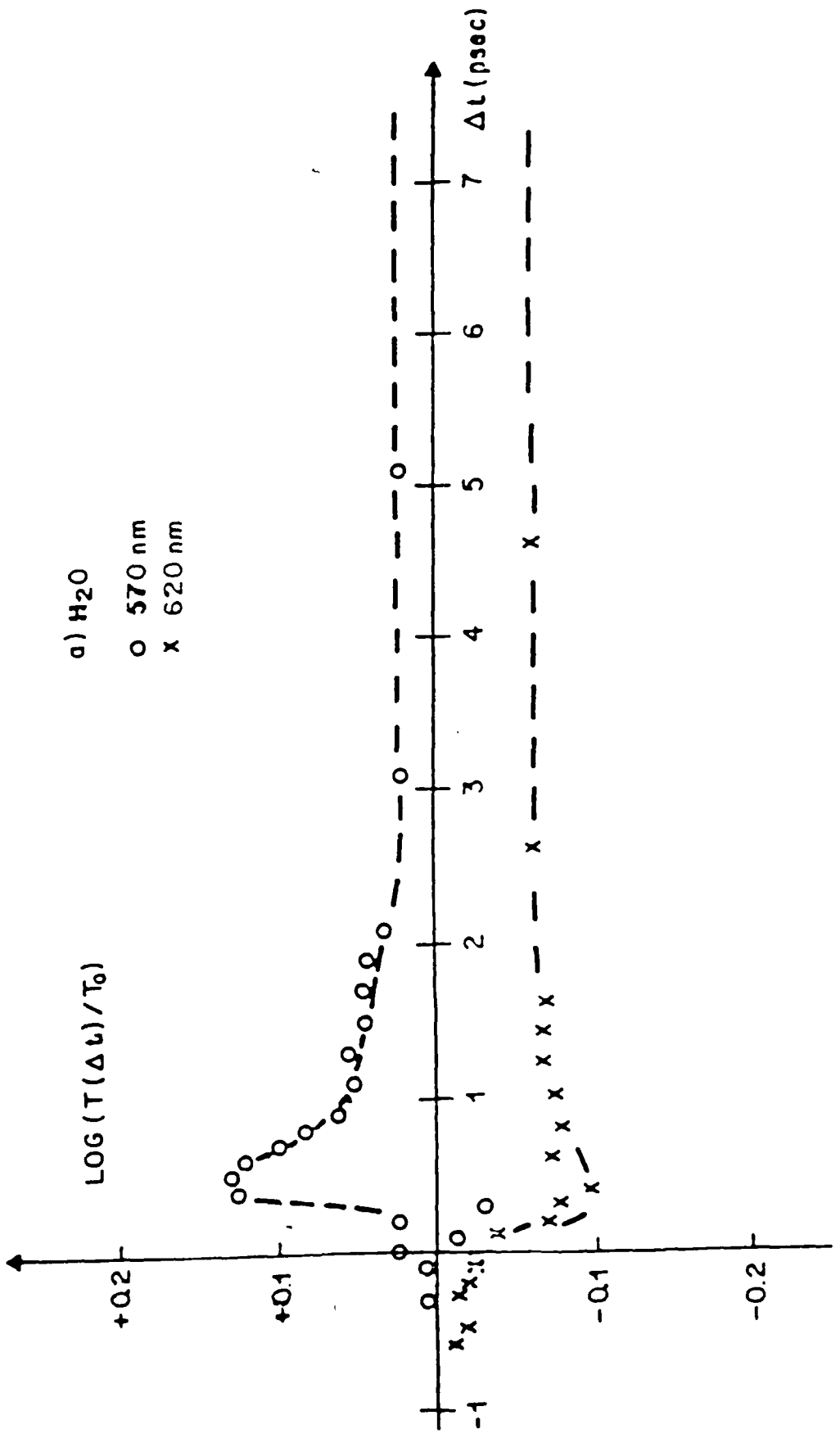
a) H2O
o 570 nm
x 620 nm
LOG (T(Δt)/T0)
+0.2
+0.1
-0.1
-0.2
-1
1
2
3
4
5
6
7
Δt (psec)

Figure 4 Response of Cone Rhodopsin in D_2O to Femtosecond Excitation. Each point is 80 fsec.

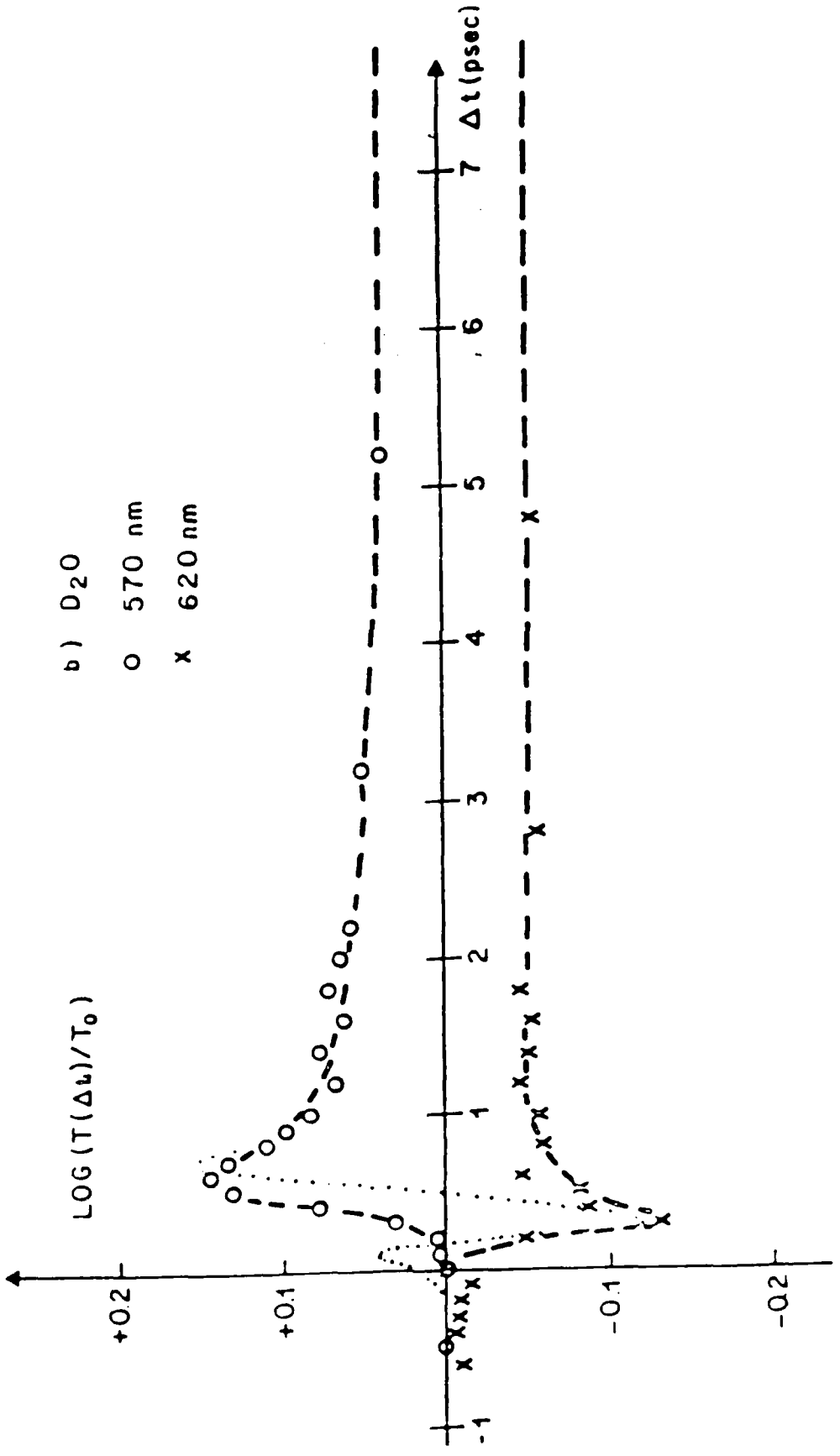
b) D_2O
o 570 nm
x 620 nm
LOG (T(Δt)/T₀)
+0.2
+0.1
-0.1
-0.2
-1
1
2
3
4
5
6
7 Δt(psec)

II. Anionic Activators of Photoreceptor Cells in the Dark

A. Introduction

As described in our last proposal, photoreceptor cells have a complex machinery for hydrolyzing under the action of light cyelic GMP and producing GMP plus a proton. This enzymatic machinery results in a large amplified response to a single photon. In essence one photon stimulates these enzymes to hydrolyze 400,000 cyclic GMP molecules to produce on a 100 msec timescale 400,000 protons. During the past two years we have been able to show that a series of anionic activators can turn on these enzymes in photoreceptor cells in the dark causing, without light, cyclic nucleotide hydrolysis (release of protons) that is normally a part of the physiological response. A surprising and startling result is that fluoride, an important additive in dental care, is among these anionic activators. It is possible that our discovery of these activators will allow us to modulate visual sensitivity and excitation.

B. Biochemical Introduction

Vertebrate retinal rod outer segments (ROS) contain a light-activated phosphodiesterase (PDE) that is highly specific for cyclic GMP (6-11). Photoexcited rhodopsin does not bind to PDE directly, but activates this enzyme via an intermediary protein called the G-protein or transducin (12). The absorption of light induces a conformational change in rhodopsin that results in the binding of the G-protein to rhodopsin (13) and the catalytic exchange of GTP for GDP on the G_α subunit of the G-protein (12). G_α-GTP dissociates from rhodopsin and the $G_{\beta\gamma}$ complex, and binds to phosphodiesterase (13). The binding of G_α-GTP to PDE results in the dissociation of the inhibitory γ subunit

of phosphodiesterase with the subsequent hydrolysis of cyclic GMP to GMP (6-11). In vitro the response of this system to light is highly amplified and is associated with visual transduction, since the absorption of a single photon results in the catalytic exchange of GTP for GTP on ≈500 G-proteins (12), and these G-proteins each activate ≈800 PDE molecules leading to the hydrolysis of 4×10^5 cyclic GMP within one second of photon absorption (7).

The activation of PDE by light has many similarities to the activation of adenylate cyclase by hormone receptors located on the surface of many types of eukaryotic cells (15). The absorption of light by rhodopsin (12) and the binding of catecholamine hormones to cell surface receptors (16) both catalyze the exchange of GTP for GDP bound to the respective G-protein of each system (15). In the adenylate cyclase system, the G-GTP complex activates the catalytic subunit of this enzyme, leading to the synthesis of cyclic AMP from ATP (16). Recently, there has been a report of a functional exchange of the components of the adenylate cyclase and ROS phosphodiesterase systems (17).

Fluoride ions (18-23) vanadate (24) and molybdate (25,26) activate membrane-bound adenylate cyclase purified from a number of different tissues, but tungstate does not activate this enzyme (25). In this paper, we demonstrate that vanadate, fluoride, molybdate and tungstate activate rod outer segment PDE in the absence of light. Since tungstate stimulates ROS PDE at low concentrations but does not activate adenylate cyclase, this anion may be employed as a selective stimulator of PDE-mediated cyclic nucleotide hydrolysis in photoreceptors and other cells.

C. Materials and Methods

All reagents were obtained from Sigma (St. Louis, MO) unless otherwise noted. Bovine retinas were obtained from American Stores (Lincoln, NE) and kept in liquid nitrogen until use. Retinal rod outer segments were isolated by conventional sucrose flotation techniques, with brief centrifugation times to avoid increasing the dark PDE activity (7). Isolation procedures were carried out at 4°C or with reagents on ice using infrared illumination (λ>750 nm) and an image convertor (NI-Tec, Inc., Niles, IL). Typically, 100 bovine retinas were removed from liquid nitrogen and thawed at room temperature for 30 minutes, followed by immersion of the vials in cool water for further thawing as necessary. Retinas were placed in 45% sucrose (w/v) in a buffer (60 mM KCl, 30 mM NaCl, 2 mM $mgCl_2$, 1 mM dithiothreitol, and 10 mM HEPES at pH 7.8) and manually homogenized by four passages through a teflon-glass test tube homogenizer (Wheaton), followed by 45-60 seconds of agitation on a tabletop vortexer operated at full speed. 32 cc of this material was placed in each of 3 cellulose nitrate tubes, overlayed with 1-2 cc of the above buffer, and centrifuged at 22K for 20 minutes in an SW 25.1 swinging bucket rotor (Beckman, Palo Alto, CA). Crude ROS harvested from the sucrose-buffer interface were diluted 4:1 with buffer and centrifuged at 5K for 20 minutes in a fixed-angle SW 30 rotor (Beckman). The resulting pellet was resuspended in 96 cc of 38% sucrose (w/v) in the above buffer, divided into 3 cellulose nitrate tubes each overlayed with 1-2 cc of buffer, and centrifuged at 22K for 20 minutes as above. Purified ROS harvested from the sucrose-buffer interface were diluted 4:1 with buffer and pelleted at 5K for 20 minutes. The pellet was resuspended in several cc of buffer, divided into

200 µl aliquots, and stored in liquid nitrogen until further use. A 10 µl aliquot of this suspension was solubilized in 1 cc of 1.5% Ammonyx LO (Onyx Chemicals, Jersey City, NJ) in 10 mM HEPES, 50 mM hydroxylamine at pH 7.8, and the rhodopsin concentration was determined by absorption difference spectroscopy using ε = 42,700 M^{-1} cm^{-1} at 500 nm. A_{280}/A_{500} was typically 1.9-2.3.

Experiments were performed at room temperature by diluting the ROS suspension to a final concentration of 4-15 µM rhodopsin. The assay mixture contained 4 mM cyclic GMP and 1 mM $CaCl_2$ in the above buffer in a total volume of 250 µl. The ROS solution was placed in a small test tube and rapidly stirred with a magnetic spin bar. For dark trials, 2.5 µl aliquots of a concentrated stock solution containing the anion of interest were added to the ROS suspension at ≈1 minute intervals, with up to 8 serial additions of anion per sample. In this manner, each ROS solution could be used to determine the PDE activity at several different anion concentrations. The number of serial additions was limited by two factors: (1) all measurements were completed before the pH changed by 0.2 units, and (2) the total added volume was limited to less than 8% of the initial volume. The effect of diluting the ROS sample by up to 8% of the initial volume was corrected for by multiplying the measured rate of cyclic GMP hydrolysis by $[(250 + \alpha)/250]^2$, where α is the volume of solution (in µl) added to the ROS suspension during the course of the experiment. This theoretical correction factor takes into account the decrease in the rhodopsin concentration of the suspension, and the attenuation of the measured pH change by the larger volume of the assay solution. The validity of using this correction factor was tested experimentally by diluting the ROS sample by

up to 8% with serial additions of 2.5 µl aliquots of buffer, and the theoretical correction factor was found to negligibly underestimate the experimentally determined value.

To determine the effect of these anions on the light-activated rate of cyclic GMP hydrolysis by PDE, the ROS sample was maximally activated by either full bleaching in room lights or exposure to a calibrated commercial photoflash unit (Vivitar) placed 20 cm from the sample. Either 40 µM GPPNHP or 1 mM GTP was added to the ROS suspension prior to illumination, since light activation of PDE requires a guanyl nucleotide cofactor (15). When bright flash illumination and a GTP cofactor were used, the initial measurement of light-activated PDE activity was made 30 seconds after the flash, since we observed that the activity of PDE remains constant for several minutes after this time. The effect of the anion of interest on light-activated PDE activity was then determined by serial additions of 2.5 µl aliquots of a concentrated stock solution of this anion, as described above.

The protons released by complete hydrolysis of 4 mM cyclic GMP led to a pH change of ≈0.7 units. This change in pH was recorded by displaying the output of a portable pH meter equipped with a microelectrode (Markson Scientific, Phoenix, AZ) on a strip chart recorder. The phosphodiesterase activity (moles of cyclic GMP hydrolyzed/second) is determined by the slope of this tracing, since hydrolysis of one mole of cyclic GMP releases one mole of H^+ at pH 7.8 (9). Buffering capacities of the individual media were determined by back titration with 0.1 N NaOH.

D. Results

Vanadate is the most potent activator of ROS PDE (K_M ≈ 100 μM), and the concentration of vanadate that maximally activates PDE in the dark is 2 mM (Figure 1). Within the error of our measurements, adding 2 mM vanadate does not significantly increase the activity of light-activated PDE. Concentrations of vanadate greater than 2 mM markedly inhibit the activity of PDE activated either by light or by lower concentrations of vanadate in the dark. The K_I value for vanadate inhibition is ≈ 6 mM. Although greater than 6 mM vandate significantly increases the buffering capacity of the ROS suspension, the measured hydrolytic velocities can readily be corrected for this effect. The inhibition of PDE activity by vanadate is unequivocal, since the decrease in hydrolytic velocity caused by > 2 mM vanadate greatly exceeds any error introduced by correcting for these buffering capacity changes. The inhibition of PDE by high concentrations of vanadate does not appear to be due to a non-specific ionic perturbation of the medium, since up to 100 mM excess NaCl inhibits the light-induced activity of PDE by less than 10% (data not shown). Fluoride exactly duplicates the results on vanadate (data not shown).

Tungstate activates PDE in the dark at higher anion concentrations than are required for vanadate or fluoride activation (Figure 2). The K_M for tungstate activation is ≈ 1 mM, and 10 mM tungstate activates PDE to nearly the same extent that this enzyme is activated by light. Up to 10 mM tungstate does not significantly increase the activity of PDE that is activated by light. Concentrations of tungstate greater than 10 mM may inhibit PDE activity stimulated either by light or by less than 10 mM tungstate in the dark. However, we cannot be certain

of the inhibitory effect of this anion because the large changes in buffering capacity produced by greater than 10 mM tungstate limited the accuracy of our measurements. If tungstate inhibits PDE at high concentrations, this inhibition is not as striking as in the case of vanadate inhibition of this enzyme.

Molybdate is the least potent of these anionic activators of PDE, since the K_M for molybdate activation is ≈ 3 mM (Figure 3). 10-20 mM molybdate maximally activates PDE in the dark, but the level of PDE activity produced by this molybdate concentration is only 30-35% of the PDE activity produced by light. 30 mM molybdate either does not inhibit or minimally inhibits PDE activated by either light or lower concentrations of molybdate. As in the case of tungstate, the change in buffering capacity produced by high concentrations of molybdate limits the accuracy with which an inhibitory effect of this anion can be determined.

Chromate, a group VI B tetroxo complex similar to vanadate, molybdate and tungstate, does not significantly activate ROS phosphodiesterase in the dark (data not shown).

In the presence of 0.5 mM ATP and 0.5 mM GTP, PDE activated by a weak flash undergoes a first order decrease in the rate of cyclic GMP hydrolysis (referred to as deactivation), with a time constant of 11-18 seconds in 10^{-9} M Ca^{++} and 28-42 seconds in 10^{-3} M Ca^{++} (11). All of the results reported in this paper on anionic activation of PDE were obtained with 10^{-3} M Ca^{++} added, to avoid any uncontrolled effects arising from small amounts of contaminating Ca^{++} in our assay. However, since flash-induced deactivation is most striking in 10^{-9} M Ca^{++},

we conducted our assay for anion-induced deactivation in low Ca^{++}. Using 10^{-9} M Ca^{++}, we observed that the phosphodiesterase activity remained constant for at least 2 minutes after addition of 1.2 mM vanadate, 0.8 mM tungstate and 2-4 mM molybdate in the presence of 0.5 mM ATP and 0.5 mM GTP in the dark. Thus, we did not obtain any evidence to suggest that anion-activated PDE undergoes an ATP-dependent deactivation similar to the ATP-dependent deactivation of PDE after a flash of light.

E. Discussion

Our results demonstrate that vanadate, fluoride, molybdate and tungstate each activate rod outer segment phosphodiesterase in the dark. Vanadate and fluoride ($K_M \approx 100$ μM) is the most potent activator of ROS PDE, followed by tungstate ($K_M \approx 1$ mM) and molybdate ($K_M \approx 3$ mM). Either 2 mM vanadate or 10 mM tungstate produces PDE activity which is > 90% of the maximal light-activated rate for this enzyme. However, 10-20 mM molybdate can elicit only 30-35% of the activity of PDE produced by light. PDE in ROS suspensions that is maximally activated by light and a guanyl nucleotide cofactor cannot be activated further by addition of vanadate, fluoride, molybdate or tungstate. High concentrations of vanadate and fluoride clearly inhibit the activity of ROS PDE elicited by either light or up to 2 mM vanadate or fluoride in the dark. High concentrations of molybdate and tungstate may also minimally inhibit PDE, but this is difficult to determine because the change in buffering capacity due to large amounts of tungstate and molybdate limited the accuracy of our measurements.

Possible Mechanism for Anionic Activation of PDE

Fluoride activates adenylate cyclase by interacting with the G-protein (20), and vanadate and molybdate may also activate this enzyme by interacting with the G-protein (26). In view of the similarities between light-activated PDE and hormone-stimulated adenylate cyclase (15,17), we would like to suggest that vanadate, fluoride, molybdate and tungstate may activate PDE by acting on the G-protein of the ROS enzyme system. Although the molecular aspects of this activation are not known, several facts suggest how these anions might stimulate ROS PDE. The chemistry of vanadate, tungstate and molybdate oxyanions is very similar to the chemistry of phosphate (27,28). Vanadate competes with phosphate for binding, and the ability of vanadate to adopt a structure similar to the transition state of phosphate may account for its ability to inhibit a wide variety of enzymes (27,29). If the G-protein is involved in the activation of PDE by these anions, a simple and elegant mechanism to explain this effect can be suggested. Since it is known that GTP must replace GDP on the G_α subunit of the G-protein in order to stimulate PDE (12,13), the presence of the terminal γ-phosphate of GTP must be crucial for the activation of PDE by light. In the absence of GTP exchange stimulated by photolyzed rhodopsin, vanadate, molybdate and tungstate (represented as A in Figure 4) may be capable of assuming a molecular configuration that mimics the presence of the terminal γ-phosphate of GTP at the guanyl nucleotide binding site of G_α. This could result in the dissociation of G_α from $G_{\beta\gamma}$ which is required for PDE activation. Interestingly, the recent demonstration that aluminum is required for the activation of adenylate cyclase by fluoride (30,31) may allow the activation of PDE

by fluoride previously reported (17,23) to be incorporated into the above scheme. Aluminum in the presence of fluoride may exist primarily as AlF_4^-, suggesting that a metal liganded with multiple fluoride ions is the species involved in activation of adenylate cyclase (30). Therefore, the activation of phosphodiesterase by fluoride may be due to the generation of a polyionic complex that can bind to the same site at which vanadate, molybdate and tungstate activate PDE.

Figure 1: Vanadate Activates Rod Outer Segment Phosphodiesterase. In the dark, low concentrations of vanadate stimulate the activity of ROS PDE, with 2 mM vanadate stimulating this enzyme to > 90% of the light-induced activity. Concentrations of vanadate > 2 mM inhibit the activity of PDE elicited by light or lower vanadate concentrations in the dark. The light curve was determined by bleaching 6% of the rhodopsin present in ROS suspensions containing 1 mM GTP as a cofactor. The effect of vanadate on the activity of PDE in ROS samples bleached in room lights was also investigated, and the results obtained were similar to the results obtained using flash illumination (results not shown). Assay mixtures contained 1 mM $CaCl_2$ and 4 mM cyclic GMP in buffer (see text). All suspensions were 10.2 μM in rhodopsin. Experiments were performed at room temperature at an initial pH of 7.8, and all measurements were completed before the pH had changed by 0.2 units. A Relative PDE Activity = 1.0 corresponds to 14.3 μM of cyclic GMP hydrolyzed/sec.

Figure 2: Tungstate Activates Rod Outer Segment Phosphodiesterase. In the dark, 10 mM tungstate stimulates the activity of ROS PDE to a level > 90% of the light-induced activity. Concentrations of tungstate

greater than 10 mM may exert a slight inhibitory effect on PDE activity, but this is uncertain because of the change in buffering capacity introduced by this anion. The effect of tungstate on the light-induced activity of PDE was determined with 40 μM GPPNHP as a cofactor, and with the sample activated by a flash bleaching 0.2% of the rhodopsin present. Assay mixtures contained 1 mM $CaCl_2$ and 4 mM cyclic GMP. Experiments were performed at an initial pH of 7.8. Suspensions were 4 μM in rhodopsin, and a Relative PDE Activity = 1.0 corresponds to 17.7 μM cyclic GMP hydrolyzed/sec.

Figure 3: Molybdate Activates Rod Outer Segment Phosphodiesterase. In the dark, 10-20 mM molybdate stimulates PDE activity to a level 30-35% of the light-induced activity of this enzyme. The effect of molybdate on the light-induced activity of PDE was determined with 1 mM GTP as a cofactor, and with the sample fully activated by bleaching in room lights. Assay mixtures contained 1 mM $CaCl_2$ and 4 mM cyclic GMP. Suspensions were 10.2 μM in rhodopsin, and experiments were performed at an initial pH of 7.8. A Relative PDE Activity = 1.0 corresponds to 11.4 μM of cyclic GMP hydrolyzed/sec.

Figure 4: Mechanism for the Anionic Activation of Phosphodiesterase. (a) In rod outer segments, the effect of light is to induce the binding of the G-protein (G) to rhodopsin (Rh), resulting in the catalytic exchange of GTP for GDP on the G-protein. G-GTP then stimulates phosphodiesterase (PDE), resulting in the hydrolysis of cyclic GMP to GMP. (b) In adenylate cyclase, the binding of hormone (H) to cell surface receptors (Rec) results in the exchange of GTP for GDP on the G-protein

of this system. G-GTP then activates the catalytic subunit (C), resulting in the conversion of ATP to cyclic AMP. (a') and (b'): Anions (A) that activate both ROS PDE and adenylate cyclase may produce their effect by interacting with the G-protein of each system. Since vanadate, molybdate and tungstate may be able to assume structures similar to the transition state of phosphate, we suggest that these oxyanions may assume a molecular configuration that mimics the presence of the terminal γ-phosphate at the guanyl nucleotide binding site on the G-protein. This could result in the activation of PDE and C by the stimulated G-protein.

Figure 1: Vanadate Activates Rod Outer Segment Phosphodiesterase

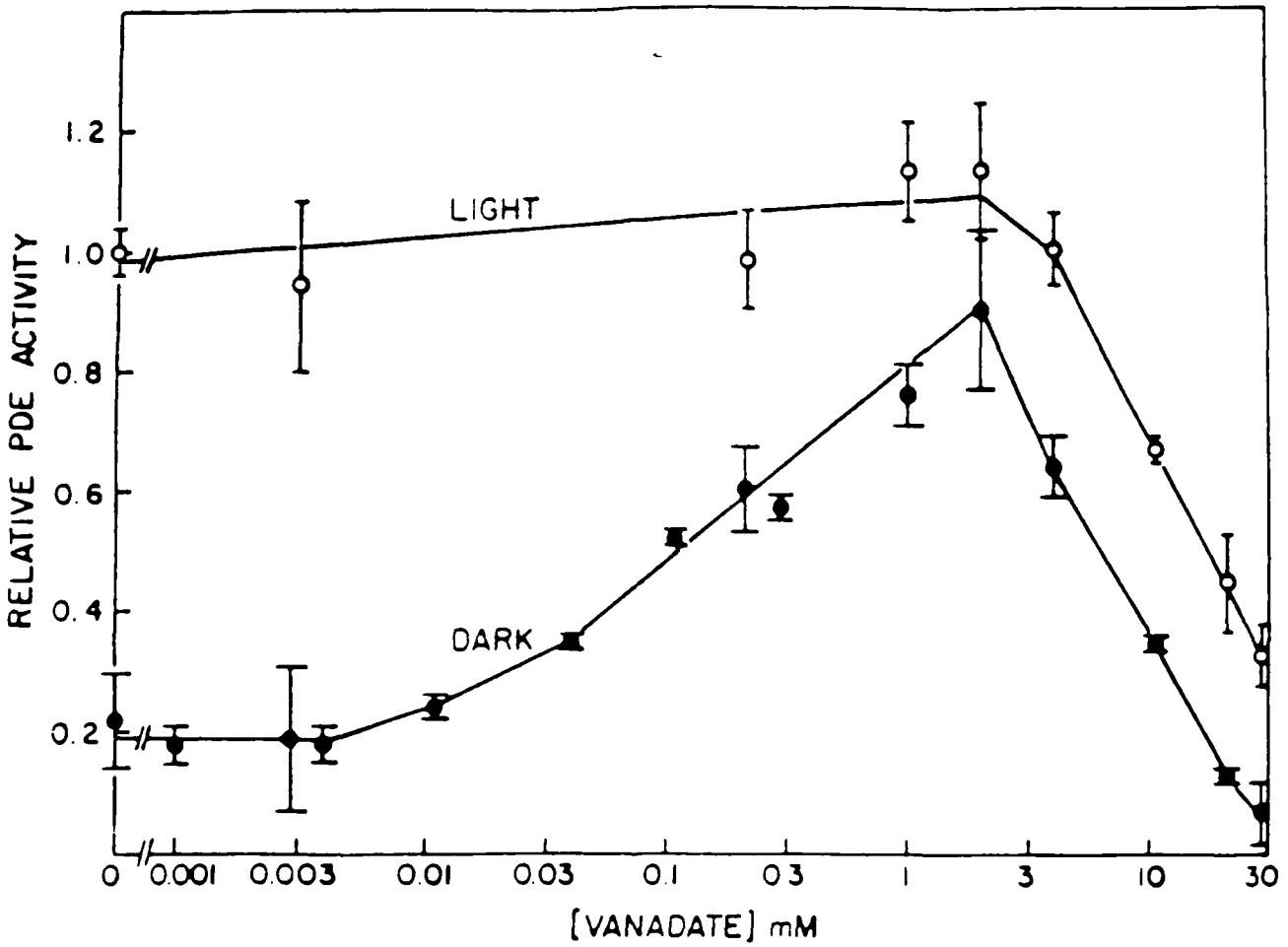

Figure 2: Tungstate Activates Rod Outer Segment Phosphodiesterase

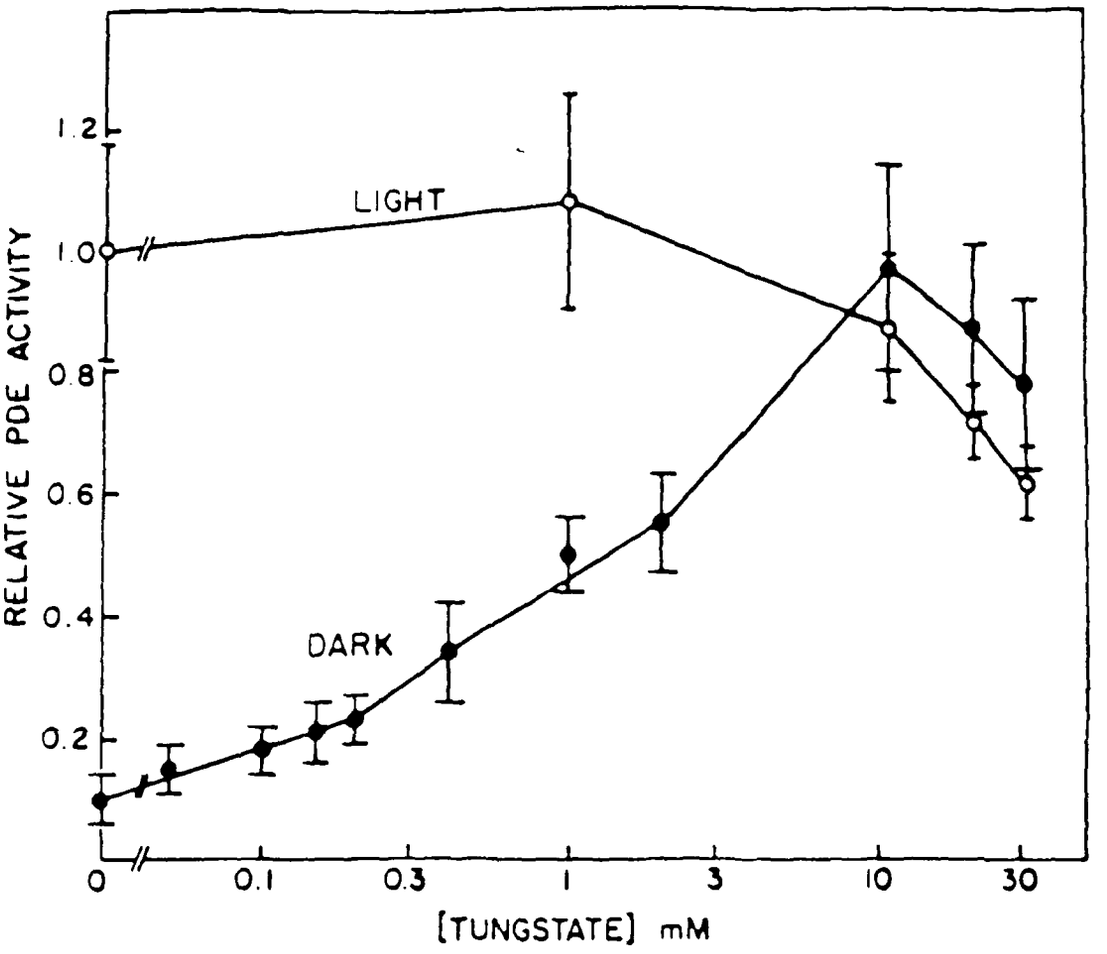

Figure 3: Molybdate Activates Rod Outer Segment Phosphodiesterase

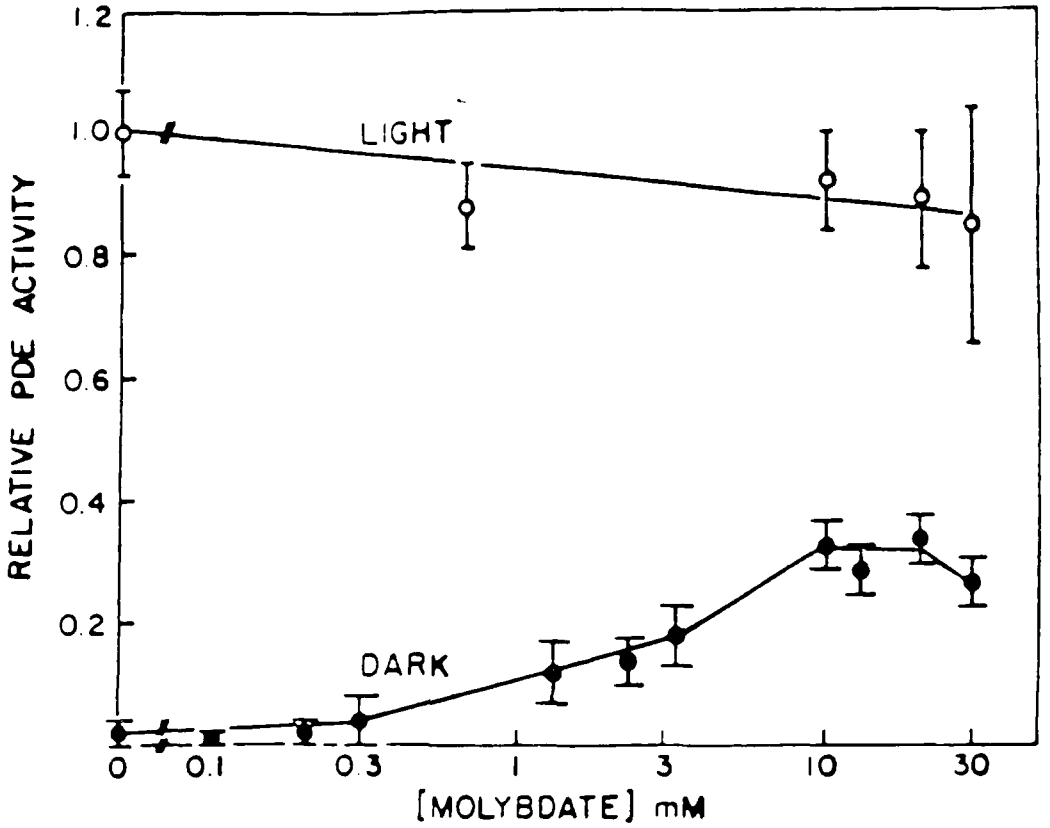

Figure 4: Mechanism for the Anionic Activation of Phosphodiesterase

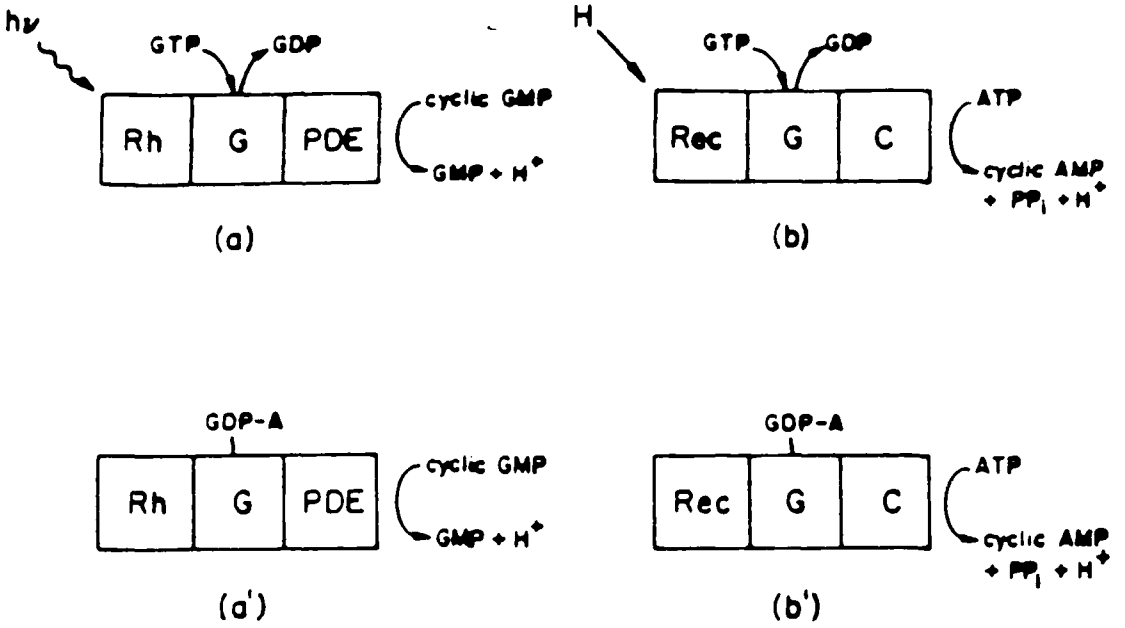

III. Oil Droplet Investigations

One of the objectives of our last proposal was to study individual turtle oil droplets as a function of size and type (red, orange or yellow). Previously (32), we had successfully studied only mixtures of oil droplets. Initially we thought that since LAIR was going to be purchasing a Raman spectrometer it would be advantageous for these studies to be completed by LAIR. I visited LAIR in June 1983 and one of the aims of that visit was to repeat on the recently installed LAIR Raman equipment our oil droplet results. This I accomplished together with Captain Cooper among several other experiments completed during my ten day stay at LAIR. The plan was for LAIR to work on a method of isolating single oil droplets in pipettes while our laboratory was to keep working with our Raman microprobe which allows the recording of a Raman spectrum through a microscope. The Raman microprobe would allow single oil droplets to be viewed and studied. On return from LAIR last summer we began to investigate the oil droplets by our microprobe method. Although we obtained data on the oil droplets we were not satisfied by the reliability of our results since there were indications that the tightly focused laser beam even with $\mu W/cm^2$ CW powers caused heating in the high optical density oil droplets. Specifically there was a broadening of the vibrational spectra and this is an internal monitor of heating. Thus over the last year we built a low temperature stage that would work with our microscope (bought several years ago on this contract) and would also be compatible with the Raman experiment.

In Figure 1 of this section our low temperature cell for Raman microprobe oil droplet experiments is shown. In this stage the sample

Figure 1 A Low Temperature Cell for Raman Microprobe Measurements of Single Oil Droplets.

Figure 2 The resonance Raman spectrum of a single red oil droplet at 77°K. Exciting laser wavelength was 488nm at 1mw of incident power. The Raman microprobe spectrum shown was recorded digitally at intervals of $2cm^{-1}$ at 10 sec per step using a Spex 1401 double monochromator, an RCA C31034A photomultiplier with photon-counting electronics and a Coherent Radiation 52G Argon ion laser. The spectrum was plotted on a Houston plotter interfaced to a PDP 11/40 minicomputer.

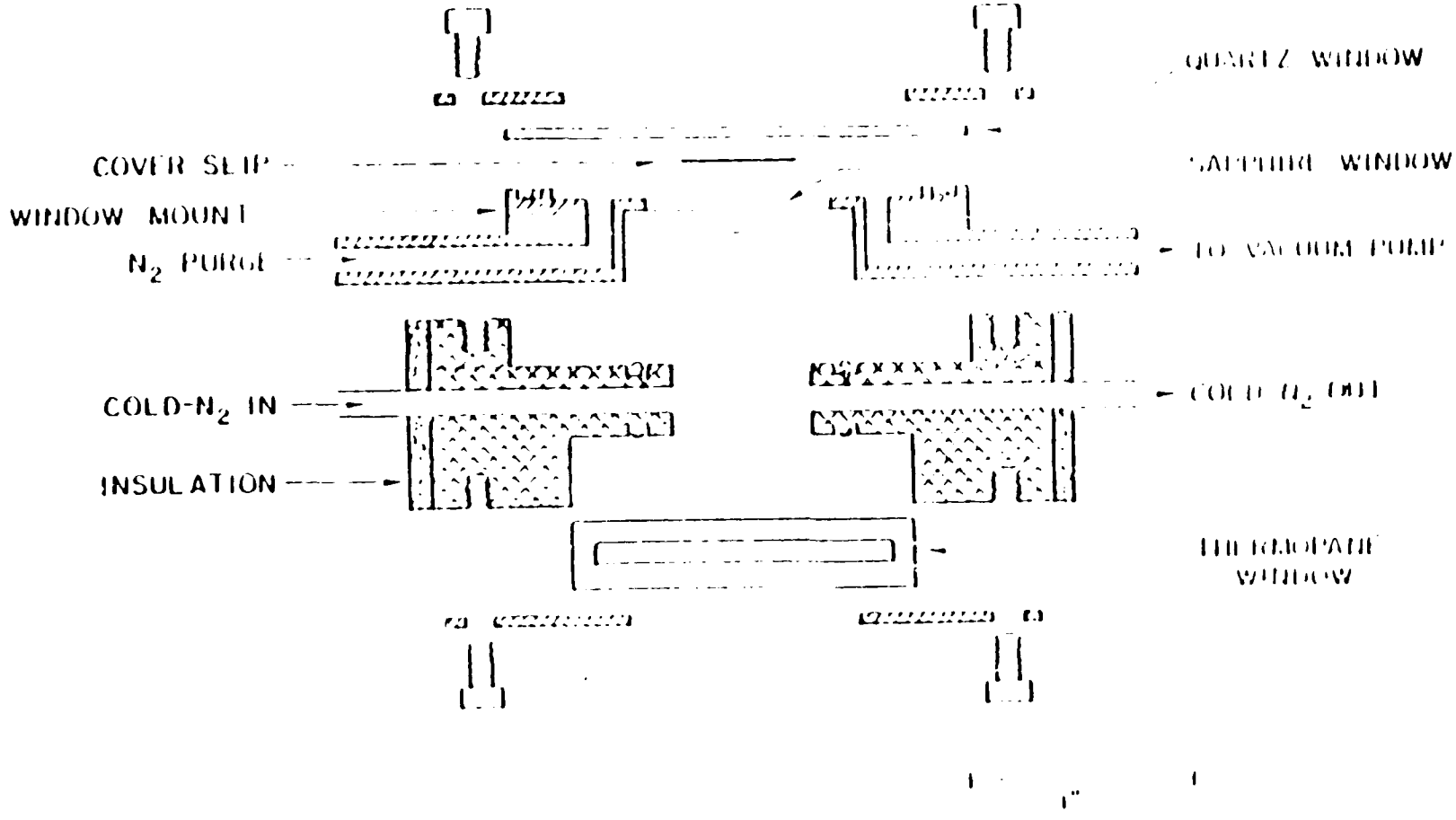
QUARTZ WINDOW
COVER SLIP
SAPPHIRE WINDOW
WINDOW MOUNT
N_2 PURGE
TO VACUUM PUMP
COLD-N_2 IN
COLD N_2 OUT
INSULATION
THERMOPILE WINDOW

Figure 1

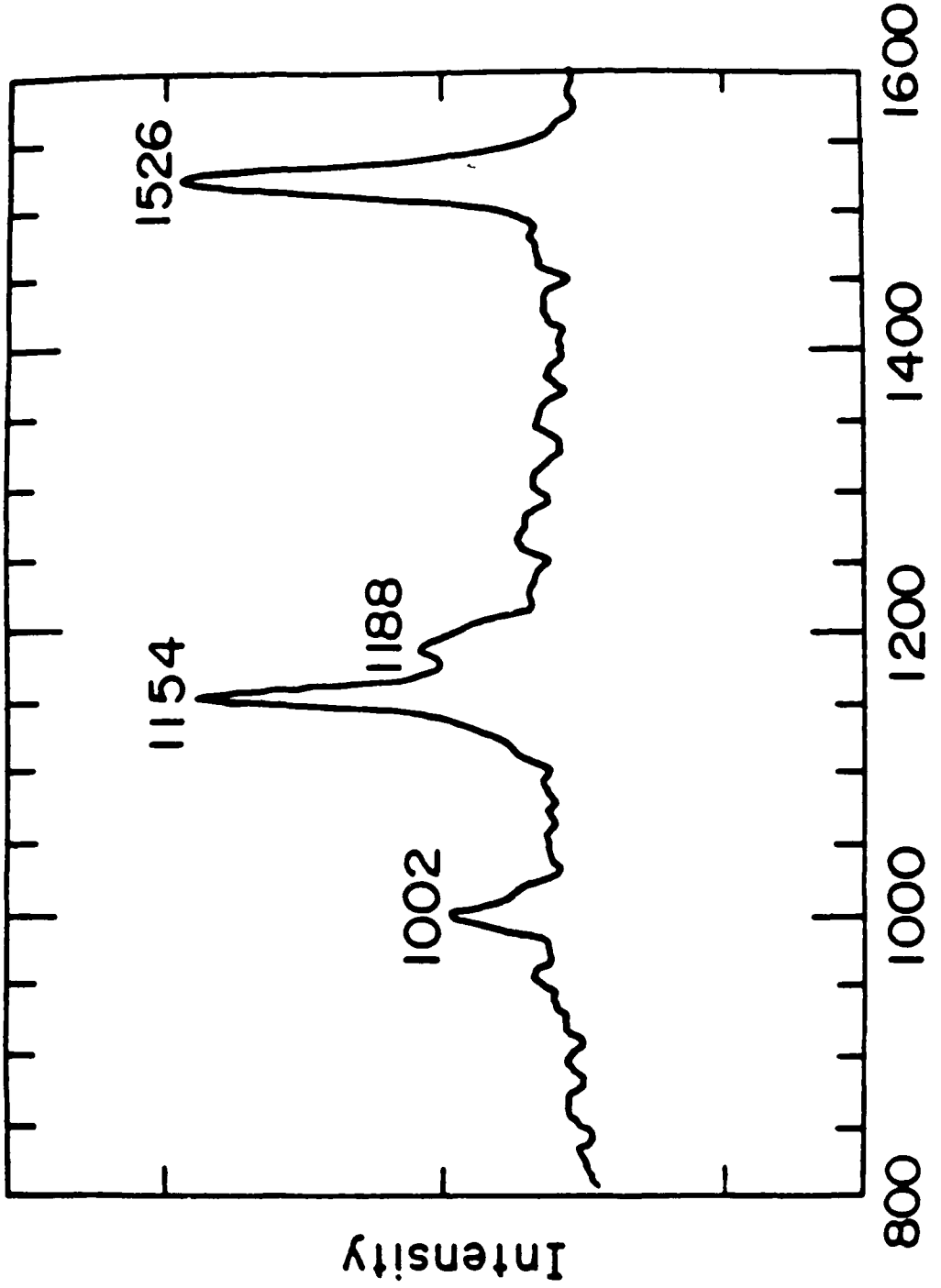
1526
1188
1154
1002
800
1000
1200
1400
1600
Frequency (cm⁻¹)
Intensity

Figure 2

is placed on a sapphire window and is covered by a cover slip. There is then a quartz window which is screwed above the cover slip but which leaves a space for purging with N_2 gas between the sample and the window. Cold N_2 is then introduced through ports in the linen-based phenolic block under the sapphire window and from the bottom an evacuated thermopane window is screwed in to provide thermal insulation.

Within the last month we have now obtained our first single oil droplet spectra from red oil droplets of the red-eared swamp turtle. The data obtained is seen in Figure 2 of this section. Based on the frequencies obtained in this resonance Raman spectrum it appears that the red oil droplet is composed exclusively of β-carotene. We are now proceeding to study some of the exciton phenomena observed earlier in the studies of oil droplet mixtures (32). The results of these studies should considerably further our goal of developing effective, rapidly altering optical filters.

IV. Elemental Localization in Photoreceptors and Other Components in Retinal, Pigment Epithelium and Choroidal Tissue

In our last proposal we described a new technique called ion microscopy via secondary ion mass spectrometry (SIMS) (33,34). This technique allowed for images to be made of specific elements in photoreceptor tissue and even isotopes of elements. In previous reviews of our work we have shown calcium images of photoreceptor cells and we were interested to determine whether the elemental composition of other pigmented components of interest to the ocular hazards program could be imaged. We have now used a procedure that allows us to image the melanin granules in the pigment epithelium and choroid together with the photoreceptor and adjacent neuronal layers.

The experimental animal used in these measurements was the toad, Bufo marinus. Eye cup preparations were used in order to develop all procedures using the eycup since LAIR measurements of laser damage are monitored in such preparations. For the measurements, toads were dark adapted for at least 2 h, then decapitated or pithed. The eye was enucleated, hemisected behind the midline, and the resulting eyecup preparation was placed in bicarbonate-buffered toad Ringer's solution. In some cases the retina was gently lifted from the underlying pigment epithelium and placed in Ringer's solution. Either preparation was then frozen in an isopentane slush cooled by liquid nitorgen. For dark-adapted conditions these manipulations were conducted under dim illumination from a Kodak Wratten II filter. Light-adapted eyecup preparations were from animals that had been in room light at least 2 h. Light-adapted isolated retinas were first removed under dark-adapted conditions and then light adapted in white room light for 10 min. All tissues were freeze-dried using a zeolite water absorbant in a vacuum established by a temperature differential. The dried materials was embedded in Spurr's low-viscosity resin under vacuum and sectioned at a thickness of 10 μm with a dry glass knife. The sections were pressed onto boron-doped silicon wafers and overcoated with 50 nm of 99.99% Au prior to analysis. Sections adjacent to the analyzed specimens were routinely examined by light microscropy in order to orient the specimen and to ensure that the area being analyzed was morphologically well preserved at the level of resolution required for these studies. The Cameca IMS 300 was operated with a positively charged oxygen primary beam of 30 nA spread over an area 250 μm in diameter. Positive secondary ions were analyzed.

Figure 1 Ion image of calcium 40 of the photoreceptor retinal layer and adjacent tissue.

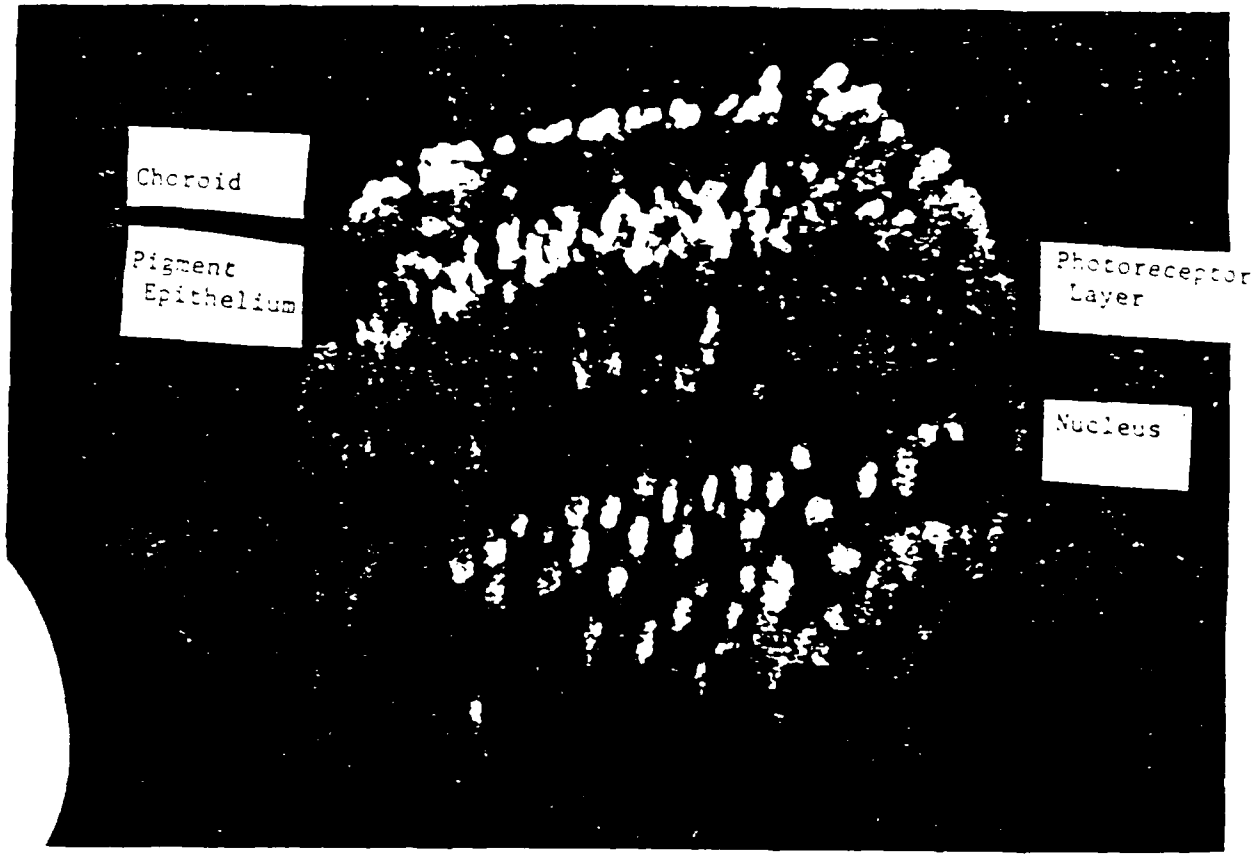
Choroid
Pigment Epithelium
Photoreceptor Layer
Nucleus

Melanin granules of both the choroid and retinal pigment epitheluim were strongly emissive for calcium (see Figure 1). Even in these light-adapted retiina, where calcium has been lost from the outer segment layer, the calcium foci between the rod outer sigments look like strung beads that are uneven in separation and interdigitatedbetween the outer segments. This almost certainly results from the distribution of melanin granules in the pigment epithelium processes, since the distribution of these calcium foci follows closely the distribution of melanin granules in pigment epithelium cells, as seen in light micrographs obtained of the same region. Calcium concentrations are also seen in Figure 1 in the inner segment and synaptic terminal layers. The procedure we used gives us hope that we will be able to study the iamges of other ions in the toad and the turtle. We also are hopeful that we will be able to study the ion images of other pigmented structures such as the oil droplets in the turtle. Since SIMS is also isotope selective we hope to be able to test the dark influx of various ions and to initiate a detailed study of parallel SIMS, electron microscopy and laser damage data in various areas of the retina and adjacent tissue.

V. Visualization of Actin in Photoreceptor Cells by Light Microscopy

A. Introduction

Over the last two years we have applied to photoreceptors the work of Barak et al.(46) on phallicidin, the actin binding toxin isolated from the fungus Amanita pholloides. Specifically this has allowed us to develop a specific stain for actin filaments in photreceptor cells. This work is particularly exciting in terms of the Ocular Hazards Program because it has allowed us, with light-microscopy to visualize this

important component of photoreceptor cells. This stain can now be universally and simply applied using the methods described in this section to analyze the effect of laser damage on this important component in photreceptors and in adjacent pigment structures such as oil droplets. It is important to note that the work reported in this section complements the pioneering studies of Enoch who developed staining procedures for the ellipsoid or mitochoudria. Therefore our stain could effectively be used in conjunction with the Enoch staining methods (58).

Rod and cone photoreceptors contain actin (38-42) in the calyceal processes (35-44) surrounding the base of the outer segment. First described in Nectarus (1), the calyceal processes are finger-like projections that arise from the apex of the inner segment and surround the base of the outer segment (35-43). In rod photoreceptors that contain scalloped discs, one calyceal process lies in each surface groove corresponding to an invagination of the discs (35,36). In humans or macaque, there are 9-12 calyceal processes per ROS, and they do not appear to be closely adherent to the plasma membrane (36). As Cohen has noted, the fact that the calyceal processes do not appear to run the length of the rod cell and are loosely applied to the membrane surface in at least some species argues against a primary role for these structures in visual transduction (36).

In teleost photoreceptors, actin filaments extend from the calyceal processes surrounding the base of the outer segment to the photoreceptor pedicle (38,40). In cone cells, these filaments extend into the inner segment, the outer fiber, around the photoreceptor nucleus, and through the inner fiber prior to inserting in the plasma membrane near the synapse (38,40). Throughout their excursion, these filaments

lie immediately subjacent to the plasma membrane. The distribution of actin filaments in teleost rods is very similar, with the important exception that filaments have not been documented in the perinuclear region. Therefore, in rod photoreceptors it is unclear if actin filaments in the inner fiber are continuous with filaments found in the inner segment.

Electron microscopy has previously been utilized to visualize actin filaments in rod and cone photoreceptors of many different species. However, although electron microscopy offer high structural detail and spatial resolution, this technique suffers from the limitations inherent in trying to reconstruct a three-dimensional view of actin filaments from multiple thin serial-sections. In addition, there is obviously no possibility of utilizing electron microscopy to visualize actin filaments in live photoreceptors. Lastly, using heavy meromyosin/subfragment-1 labeling procedures to identify actin raises the possibility of polymerization of ambient G-actin during the extended glycerination treatment (35).

Actin localization techniques utilizing fluorescently-labeled phallicidin circumvent these difficulties. Phallicidin is a potent toxin isolated from the fungus Amanita phalloides that selectively binds to and stabilizes F-actin in plant and animal cells (35-49). G-actin oligomers also bind phallicidin, but G-actin monomers do not. The three-dimensional arrangement of F-actin filaments in cells can be observed in the light microscope by staining these filaments with phallicidin conjugated to a fluorescent label. Brief fixation procedures, permeabilization of live cells by lysolecithin treatment and vesicle fusion techniques can all be used to introduce phallicidin into cells

with a minimum amount of fixation artifact. Fluorescently-labeled phallicidin has previously been used to label actin in fixed tissue culture fibroblasts (48), live mouse myoblasts (47), algae (48), conifer roots (35), metaphase spindles in rat kangaroo cells (36) and stress fibers in vascular endothelial cells (49).

In these experiments we have used rhodamine-phallicidin (Rhod-Ph) to obtain a three-dimensional view of fluorescently-labeled actin filaments in isolated rod photoreceptors and photoreceptors attached to the retina. Our results confirm the presence of actin filaments in the calyceal processes surrounding the base of the outer segments. These filaments are continuous with longitudinally-oriented filaments that lie beneath the plasma membrane in the ellipsoid and myoid regions of the inner segment. In addition, we have localized actin at the base of the outer segment in fibers oriented perpendicular to the long axis of the rod photoreceptor.

B. Materials and Methods

Bufo marinus toads 4-6 cm in length of either sex were obtained from Lemberger Associates(Germantown, WI). Toads dark adapted for at least 10-12 hours were decapitated and the eye globe was rapidly enucleated using either infrared illumination ($\lambda > 750$ nm) and an image convertor(Ni-Tec, West Jarvis, IL) or dim red illumination. The enucleated eye was hemisected just posterior to the ora serrata, and the retina was gently lifted away from the pigment epithelium with fine forceps. The retina was placed in 200 µl of a modified Ringer's solution (65 mM NaCl, 50 mM $NH_2OH \cdot HCl$, 2.5 mM KCl, 10 mM (N-2-hydroxyethylpiperazine-N'-2-ethanesulfonic acid (HEPES), 2 mm $MgCl_2$, 1 mM

$CaCl_2$, 5 mM glucose, pH 7.5-7.8), and rod outer segments (ROS) were isolated by swirling the retina for 30-60 seconds. The purpose of substituting $NH_2OH.HCl$ for NaCl was to decrease the autofluorescence of outer segments arising from the photoproducts of rhodopsin (52). Retinal fragments that remained after the detachment of the outer segments were prepared sliced into thin strips with a sharp knife with the aid of a dissecting microscope. Dim red illumination was used in this step, as the infrared image convertor was not interfaced with the dissecting microscope. Retinal fragments with outer segments attached were prepared by avoiding the ROS isolation step described above.

Some of the ROS suspensions or retinal fragements were fixed in 3.7% formaldehyde for 30-60 minutes. Unfixed ROS suspensions were permeabilized by freezing at -10°C for 20 minutes followed by thawing at room temperature. However, the morphology of the cells was inferior to the formaldehyde-fixed cells. Staining was carried out by transferring 50-100 µl of the ROS suspension or 1-2 retinal fragments to a glass slide and incubating with 50 µl of 150 ngml of fluorescently-labeled phallicidin for >20 minutes. Phallicin labeled with 7-nitrobenz-2-oxa-3 diazole(NBD)(Molecular Probes, Junction City, OR) or rhodamine demonstrated similar labeling, but rhodamine label gave superior photographs since autofluorescence from the rod cells partially obscured the fluorescence from NBD-phallicidin. Photographs were taken with a 35 mm camera(Olympus OM-2, Woodbury, NY) and a Nikon Optiphot microscope equipped with an episcopic fluorescence attachment and a mercury lamp excitation source. For Rhod-Ph, a dichroic mirror was used to select an excitation wavelength at 535-550 nm, and a 580 nm barrier filter was used to block the exciting light. Results were confirmed with NBD-

phallicidin using an excitation wavelength of 450-480 nm and a 515 nm barrier filter for viewing.

C. Results and Discussion

Figure 1 shows a low-magnification view of formaldehyde-fixed toad rods detached by shaking the isolated retina in modified Ringer's solution. Although such preparations typically contain >90% isolated outer segments, rod cells with inner and outer segments attached were present in sufficient numbers that they could easily be located for fluorescence microscopy. Figure 2 shows fluorescence and phase contrast micrographs of a cone cell exhibiting prominent staining of actin filaments by rhodamine-phallicidin. In some cells the filaments appeared to be associated as doublets but this was an inconsistent finding. In all photoreceptor cells that had inner segments attached, individual filaments originating at the scleral end of thecalyceal processes surrounding the base of the outer segment extended into the inner segment. The vitreal extent of these filaments was variable from cell to cell. In some photoreceptors, the filaments clearly run from the calyceal processes to the vitreal end of the inner segment myoid and end at the photoreceptor nucleus. Our isolation procedure paid special attention to cone cell preservation because of the importance of these cells to the Ocular Hazards Program. As can be seen in these pictures, our method clearly is applicable to these cells.

Actin filaments in each of these locations were not equally well-preserved by our formaldehyde fixation. The filaments with the calyceal processes and ellipsoid were exceptionally well-preserved, as they were always present in our preparations and appeared as thick lines of fluorescent stain (Figures 2-3). The appearance of the filaments in

the myoid region was much more variable, ranging from thick individual filaments similar to the ellipsoid filaments to a diffuse, reticular staining pattern that probably represents disrupted filaments.

In rod cells attached to the retina, filament extending from the scleral side of the nucleus into deeper retinal layers are also evident (Figure 5). Since some of these fibers appear to make an abrupt 90° turn just scleral to the ucleus (Figure 5), we are fairly confident that these represent actin filaments extend to axon of rod photoreceptors (36). Staining of actin filaments within deeper retinal layers was frequently observed, and the staining pattern was highly suggestive of the presence of actinfilaments oriented transverse to the long axis of the rod cells (Figure 3). It is not clear if all of these filaments are within Henle's fibers, or if they are located within deeper retinal layers. Studies are progressive to differentiate this staining by sectioning.

Outer segments detached from the retina by mechanical agitation separate from the inner segment at the thin connecting cilium. During this breaking process, it is possible for the calyceal processes to remain associated with either the inner segment or the outer segment. We frequently observed calyceal processes remaining associated with the outer segments (Figure 2). This was highly variable, however, as outer segments with no calyceal processes attached and inner segmentfragments with calyceal processes attached were also observed. The fact that calyceal processes can adhere to the outer segment after the inner segment is detached is somewhat surprising, since the calyceal processes

are evaginations of the inner segment. In fact, Borwein (53) has recently observed that the calyceal processes of Rhesus monkey do not remain with the outer segments during isolation procedures. Our results suggest that the calyceal processes frequently adhere to the outer segment in Bufo marinus. The discrepancy between these two results may be due to species differences.

Our photographs suggest that the actin filaments in the inner segment are closely applied to the plasma membrane. By changing the depth of focus, we could visualize the three-dimensional orientation of these filaments as well as the curvature of the plasma membrane. In all cases, the filaments appear to follow the curvature of the plasma membrane very closely, but we cannot discern whether these filaments are superficial or deep to the plasma membrane of the inner segment. Figure 5 presents a unique view that further demonstrates that the actin filaments are located in the periphery of the inner segment. A retina with rod outer segments detached was cut into small fragments, fixed in formaldehyde, and stained with rhodamine-phallicidin. A top view of the scleral side of the retina is shown in Figure 6. The solid orange circles represent the non-labeled cytoplasm of the inner segment. The bright yellow rings of rhodamine-phallicidin labeling represent a cross-sectional view of actin filaments, and these filaments are clearly located at the periphery of the inner segment. Our observations are consistent with transmission electron micrographs indicating that the actin filaments lie immediately to the plasma membrane of the inner segment (38-42), and scanning electron micrographs demonstrating prominent ridges in the inner segment membrane that may be continuous with the calyceal processes (54).

We frequently observed a prominent actin band at the junction of the inner and the outer segment oriented transverse to the long axis of the rod cell. In several isolated rods detached at the connecting cilium, this band remained associated with the outer segment. This may correspond to the labeling of the lip-like expansion of the connecting cilium at the base of outer segments reported while this work was in progress (44). In view of this localization of actin, Chaitin et al. (44) have suggested that this protein may be involved in disc morphogenesis and vectorial transport of opsin and other membrane proteins.

The rhodopsin-containing discs of the ROS have long been felt to be physically (36), electrically (55), and osmotically (56) isolated from the ROS plasma membrane. However, workers in two laboratories have recently demonstrated the presence of multiple filaments interconnecting the discs to one another and to the plasma membrane (50,51). Although the composition of these filaments is not known, it is possible that they may play a significant role in visual transduction (50,51,57). If the filaments are composed of F-actin, we would expect labeling of these structures by rhodamine-phallicidin. However, in experiments utilizing either formaldehyde-fixed ROS or ROS permeabilized by freezing and thawing, no labeling of these outer segment filaments was observed. While it may be argued that the autofluorescence arising from ROS (Figure 3) could easily obscure actin labeling in the outer segment, we do not believe this to be the case in our experiments. The amount of autofluorescence arising from formaldehyde-fixed ROS in hydroxylamine was highly variable, and on occasion no detectable autofluorescence was observed. For example, in Figure 3 there is no back-

ground fluorescence emanating from the outer segment, and no labeling of the ROS by rhodamine-phallicidin.

For several reasons, we are certain that Rhod-Ph was able to enter the outer segment under our experimental conditions: (1) the intracellular actin present in the calyceal processes and the inner segment were heavily labeled by Rhod-Ph; (2) whole rod cells with clear breaks in the plasma membrane (see Figure 3) do not demonstrate labeling with Rhod-Ph in the vicinity of the break; and (3) short, broken outer segment fragments do not show any Rhod-Ph labeling at the apical end of the cell. Therefore, either the filaments observed in ROS (50,51) are not composed of F-actin, or these filaments are not well-preserved by our fixation procedures. Burnside and coworkers have previously noted that although the calyceal and ellipsoid filaments were well-preserved, rod myoid filaments were easily disrupted and often could not be observed in fixed photoreceptors. These myoid filaments also showed variable preservation in our own experiments. The fact that we observed these labile myoid actin filaments decreases the probability that the disc-to-disc and disc-to-membrane filaments are composed of F-actin but were not well-preserved in our preparations. However, we cannot completely rule out the possibility that these filaments are actin and were not observed with our techniques.

D. Summary

We have utilized rhodamine-phallicidin to visualize actin in toad rod photoreceptors by fluorescence microscopy. Actin within the calyceal processes surrounding the base of the outer segment allow these structures to be viewed by light microscopy for the first time. In

Figure 1: Low magnification view of well-preserved toad photoreceptors 30-60 minutes after isolation.

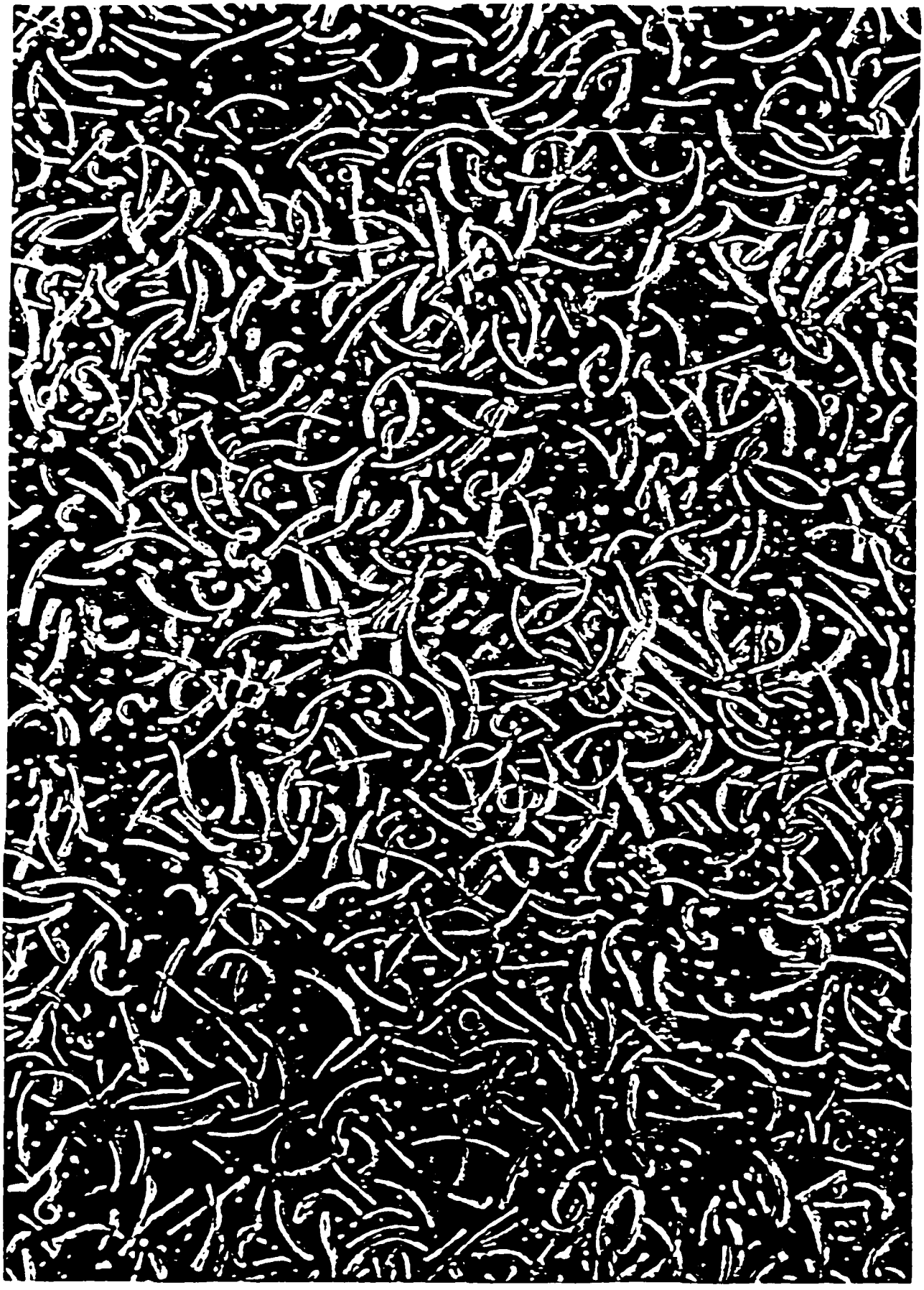

Figure 2: Phase contrast (first) and fluorescence microscopy (second) of fixed toad cone photoreceptors stained with rhodamine-phallicidin. The calyceal processes surrounding the base of this truncated outer segment appear to be associated as doublets, although this was an inconsistent finding from cell to cell. Actin staining is evident as a thick band at the right margin of the nuclus (compare first and second photographs).

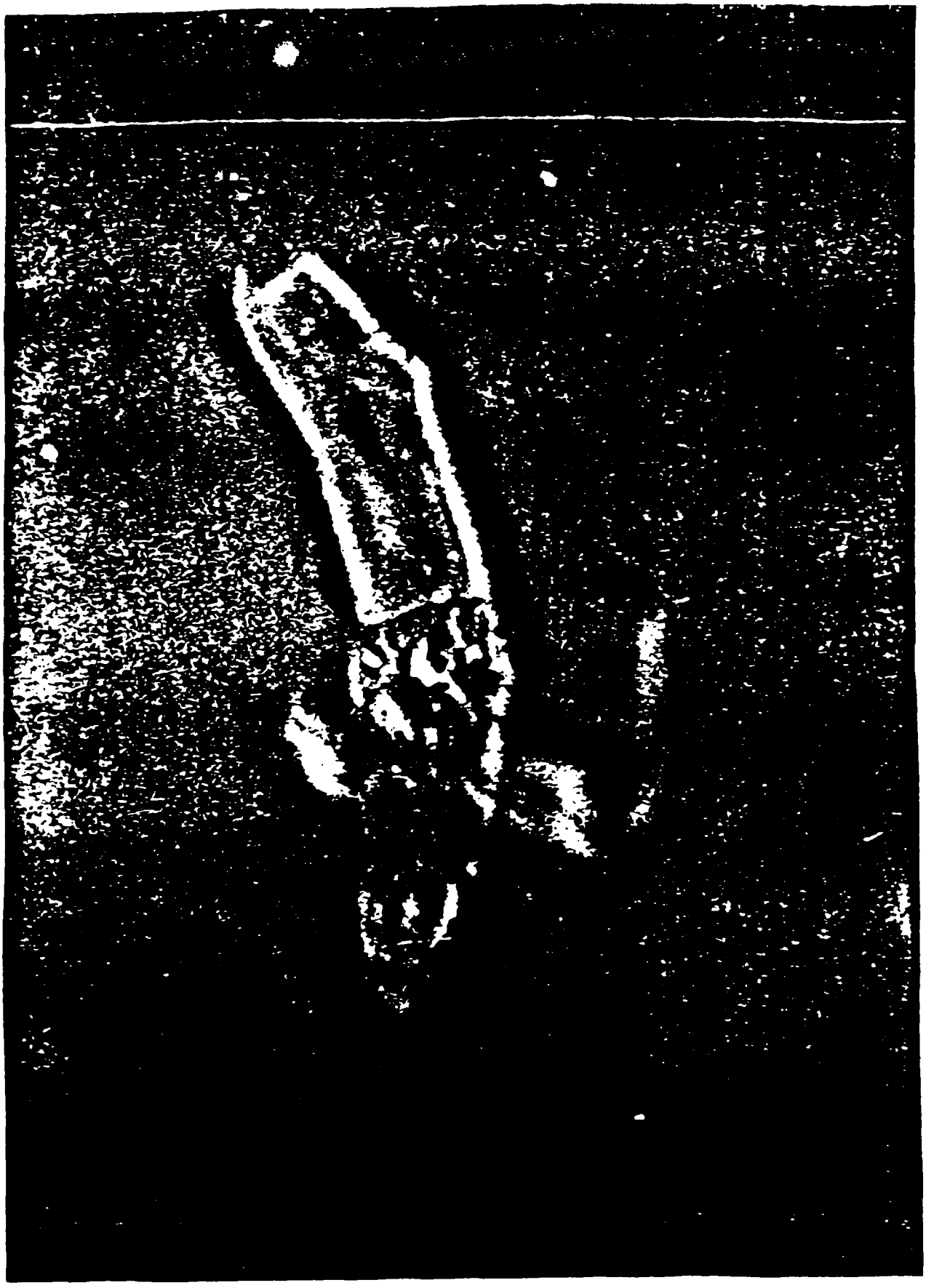

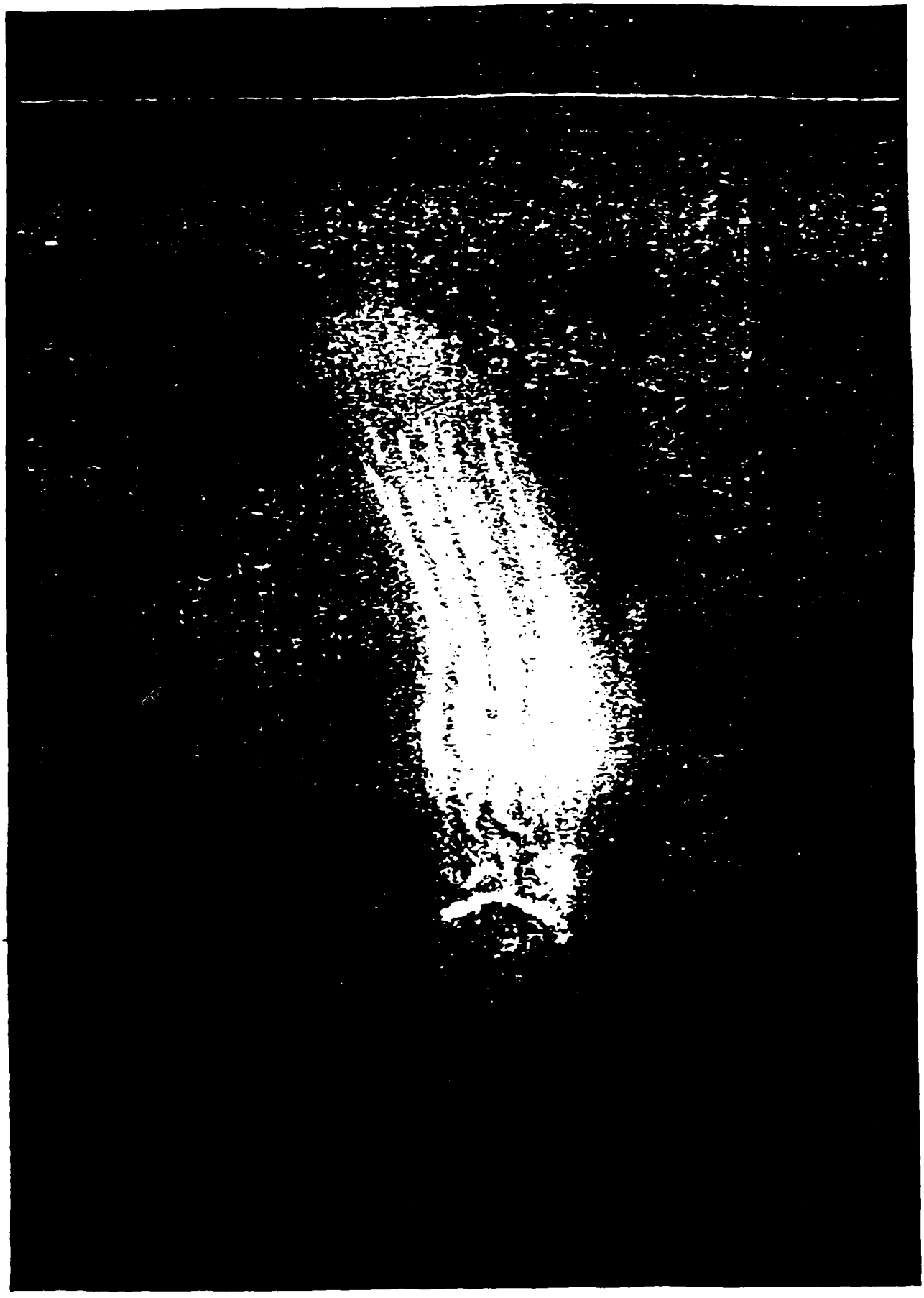

Figure 3: Phase(first) and fluorescence (second) micrographs of fixed toad rod outer segments. In the lower photograph, note the transverse band of actin staining at the base of the outer segment. Also note that a portion of the outer segment was broken during the isolation procedure (first photo), and that there is no staining of the region of the outer segment at the margins of this break by rhodamine-phallicidin. This suggests that (1) there is no actin acessible in the dark outer segment, or (2) any F-actin present in the drk is extremely liabile to the fixation procedures employed.

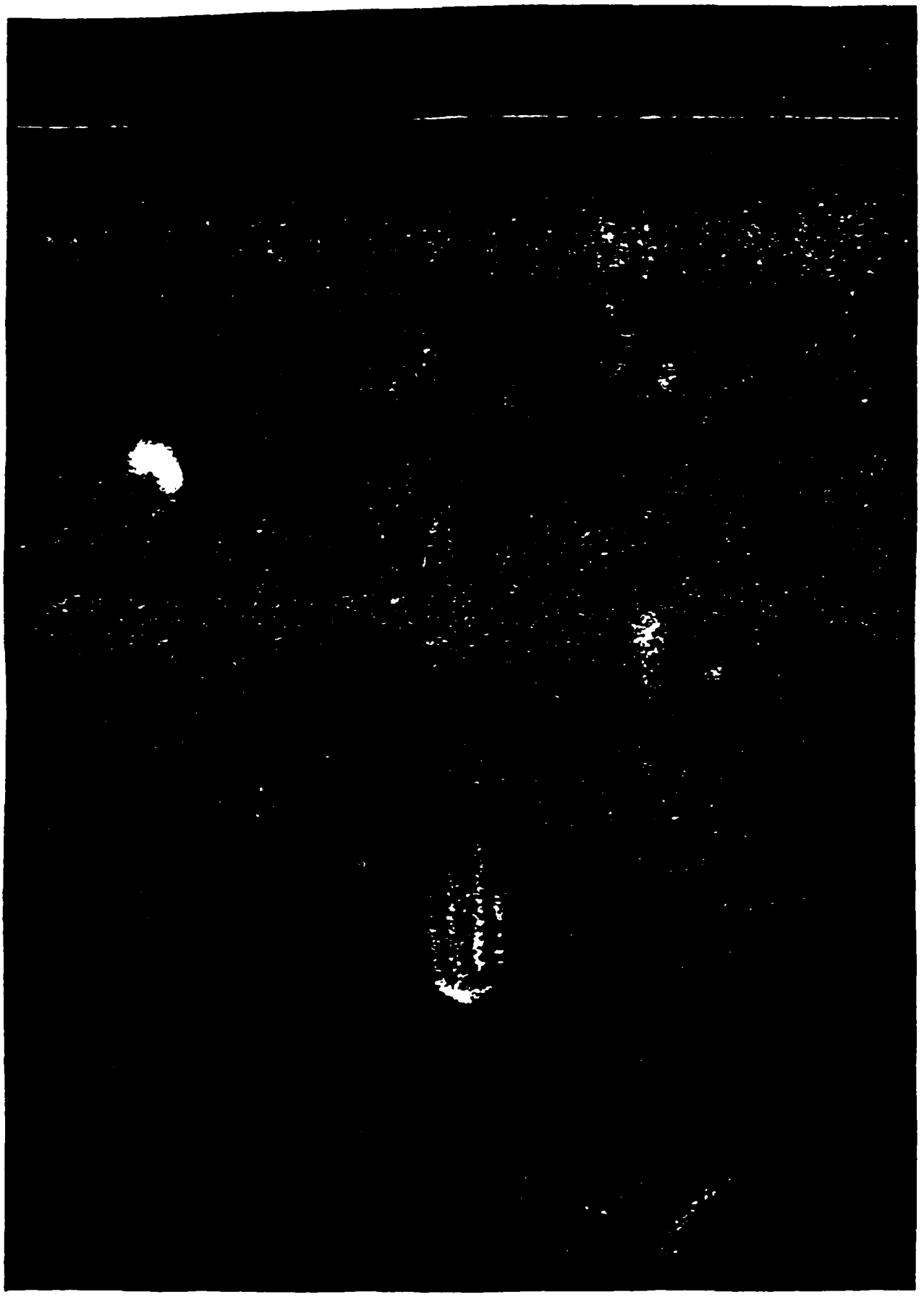

Figure 4: These toad rod outer segments are clearly detached from the inner segment by breakage at the connecting cilium. The point of this photo is to demonstrate that the calyceal processes can remain associated with the plasma membrane of the outer segment after the inner segment has been removed. First photo (phase), second photo (fluorescence).

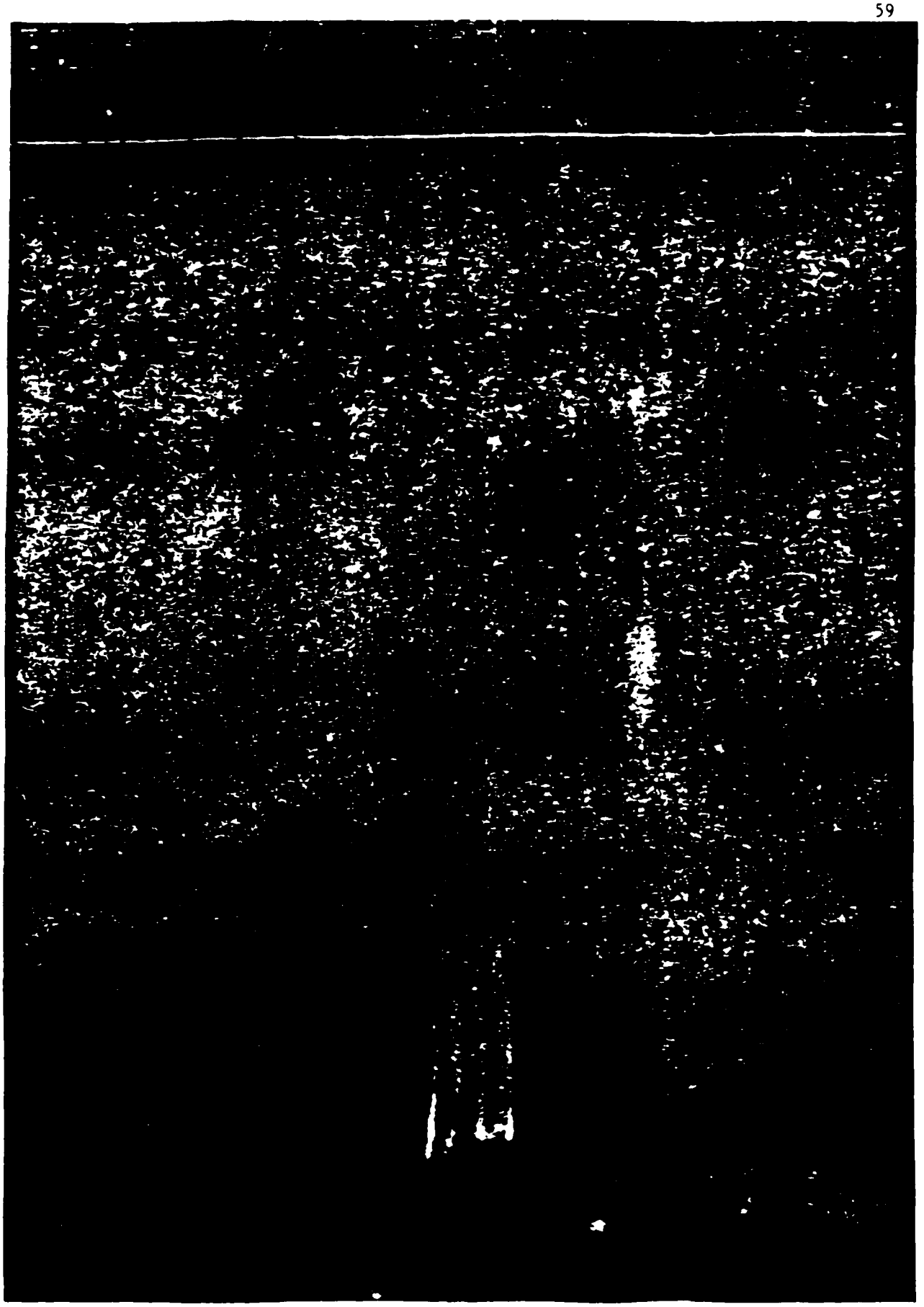

Figure 5: Toad rod photoreceptor attached to the retina: These photos clearly demonstrate the staining of actin filaments in the calyceal processes (of stain) and inner segment. The vertical line at the extreme right of the lower photo may represent actin within the photoreceptor inner fiber. First photo (phase) second photo (fluorescence).

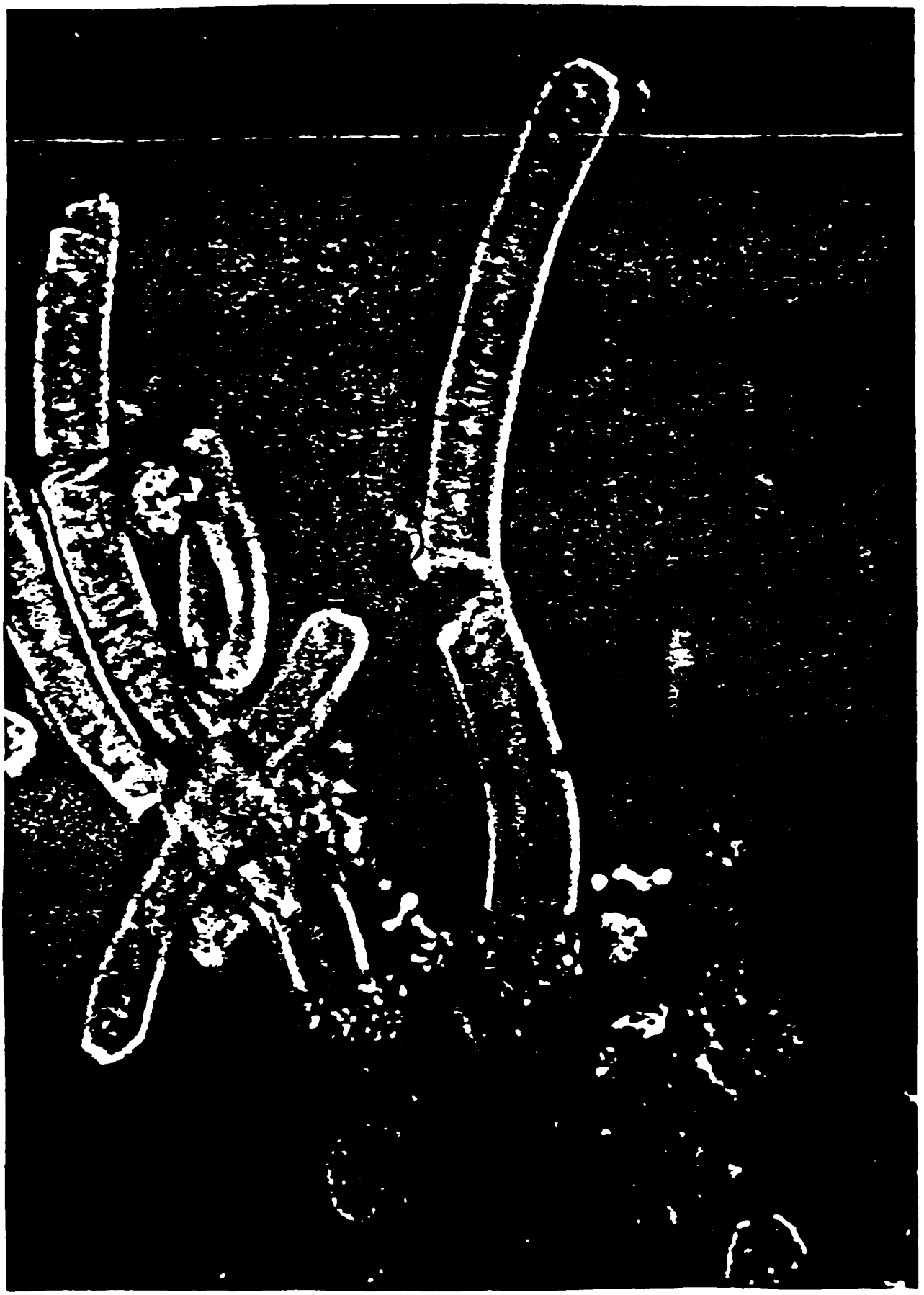

Figure 6: Cross-sectional view of the scleral side of a fixed, stained retina with photoreceptor outer segments detached. Diffuse orange is due to retinal autofluorescence, and the bright yellow rings represent circle of actin peripherally located in the photoreceptor inner segment.

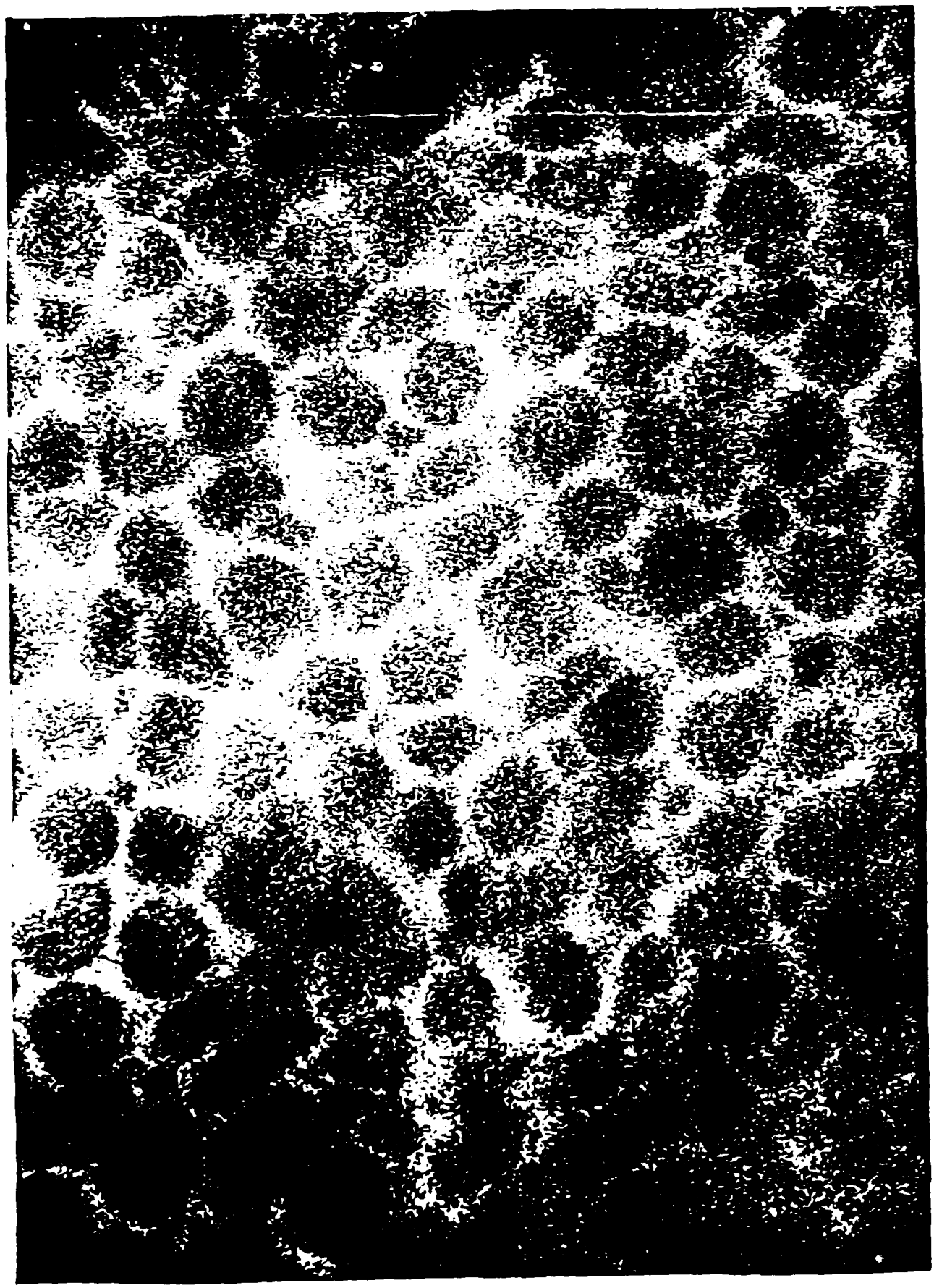

toads, the calcyceal processes frequently adhere to the plasma membrane at the base of outer segments that have been detached from the inner segment at the connecting cilium. Actin filaments clearly extend from the calyceal processes to the photoreceptor nucleus, and another series of filaments are observed in the inner fiber. We do not have any evidence suggesting that the actin filaments in the myoid are continuous with the filaments within the photoreceptor axon, although this is apparently the case in cone photoreceptors of teleost. We have also observed staining in deeper retinal layers of actin filaments oriented transverse to the long axis of photoreceptors; this may be due to actin located in photoreceptor inner fibers. Lastly, the cross-sectional photograph of the neural retina with outer segments detached shown in Figure 4 provides a unique view of actin filaments peripherally located in the photoreceptor inner segments.

Our results provide a technique for visualizing the three-dimensional structure of actin filaments in photoreceptors by light microscopy copy with a minimum of sample preparation. In addition, it should be possible to apply these fluorescent labeling techniques to living cells. Phallicidin can be introduced into live animal cells by permeabilizing the plasma membrane with lysolecithin (14) or by pinocytosis (13). Since fluorescent dye can be introduced into rod cells by vesicle fusion (20), it is possible that actin can be fluorescently labeled by these techniques in intact functioning photoreceptors.

VI. Rapid Mechanical Motions Induced by Light

One of the most surprising and significant observations made during the last year has been the observation of rapid mechanical

motions in photoreceptor cells that parallel the cellular electrophysiological response (59). The key to measuring these rapid machancial motions is a piezoelectric crystal made of lead-zirconate-titanate. This crystal converts mechanical motion into an electrical signal which can be amplified and recorded. Attached to this piezoelectric device is a finely tapered stylus which rests on a 6μ toad photoreceptor cell. The cell which is coupled to a retina, kept alive with appropriate media, is placed between two plastic rings that separates two compartments of the culture media. This allows simultaneous recording of the electrical and mechanical response. The photoreceptor is then exposed to a msec flash of light which is represented by the horizontal bar in Figure 1B. This causes a short push of the cell against the stylus (see Figure 1A) and then a prolonged pull and recovery that follows the electrophysiological response. The vertical bar is what a 1 μg response would cause. Recently, we have obtained preliminary data indicating that the mechanical response is affected by the state of light-adaption of the cell in the same way as the electrical signal is affected. We are presently investigating this more thoroughly. Within the last few months a group at Woods Hole has obtained very similar results of rapid mechanical motion in the invertebrate retina of squid (60). They also observe that the mechanical motion parallels the electrophysiological response and is a function of the state of light-adaption of the cell.

All of this data together with our actin labelling results strongly suggest that photoreceptor cells not only have rapid biochemical changes to light but also have rapid light-induced mechanical responses. We do not know yet which is the horse and which is the cart in

this evolving story but these results we believe have enormous implication to understanding laser interactions with photoreceptors. We plan to do critical experiments to evaluate the effects of CW and pulsed laser exposure to our rapid responses. These experiments will be completed in consultation with Col. Beatrice and the LAIR staff. The data will surely lead to new understandings of importance to the Ocular Hazards Program.

Figure 1 Mechanical (A) and electrophsiological (B) responses of a toad photoreceptor cell. The vertical bar in A represents a 1 µg mechanical response and the horizontal bar in B represents a 7 msec flash of light that presents the retina at 500 nm with 15 $\mu W/cm^2$.

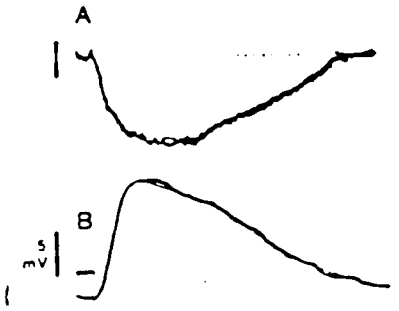
A
B
3.5 mV

BIBLIOGRAPHY

1. R.L. Fork, C.V. Shank, R. Yen and G.A. Hirlmann, IEEE Journal of Quantum Electronics QE 19, 500 (1983).
2. M.D. Hirsch, M.A. Marcus, A. Lewis, H. Mahr and N. Frigo, Biophys. J. 16, 1399 (1976).
3. E.W. Abrahamson, NIH Visual Pigment Conference (1972) p. 211.
4. E.P. Ippen, C.V. Shank, A. Lewis, M.A. Marcus, Science 200, 1279 (1978).
5. A. Lewis, Proc. Natl. Acad. Sci. (U.S.A.), 75, 549 (1978).
6. Liebman, P. A. and Pugh, E. N., Jr. (1979) Vision Research 19, 375-380.
7. Yee, R. and Liebman, P. A. (1978) J. Biol. Chem. 253, 8902-8909.
8. Liebman, P. A. and Pugh, E. N., Jr. (1980) Nature 287, 734-736.
9. Kawamura, S. and Bownds, M. D. (1981) J. Gen. Physiol. 77, 571-591.
10. Polans, A. S., Kawamura, S. and Bownds, M. D. (1981) J. Gen. Physiol. 77, 41-48.
11. Del Priore, L. V. and Lewis, A. (1983) Biochem. Biophys. Res. Commun. 113, 317-324.
12. Fung, B. K. K. and Stryer, L. (1980) Proc. Natl. Acad. Sci. U.S.A. 77, 2500-2504.
13. Kuhn, H. (1981) in Current Topics in Membrane and Transport (Miller, W. H., ed.) Vol. 15, pp. 171-201, Academic, New York.
14. Hurley, J. B. and Stryer, L. (1982) J. Biol. Chem. 257, 11094-11099.
15. Pober, J. S. and Bitensky, M. W. (1979) Adv. Cyclic Nucleotide Res. 11, 265-301.

16. Levitsky, A. (1981) C.R.C. Critical Reviews in Biochem. 10, 81-112.

17. Bitensky, M. W., Wheeler, M. A., Rasenick, M. M. Yamazaki, A., Stein, P. J., Halliday, K. R. and Wheeler, G. L. (1982) Proc. Natl. Acad. Sci. U.S.A. 79, 3408-3412.

18. Rall, T. W. and Sutherland, E. W. (1958) J. Biol. Chem. 232, 1065-1076.

19. Howlett, A. C., Sternweiss, P. C., Macik, B. A., Van Arsdale, P. M. and Gilman, A. G. (1979) J. Biol. Chem. 254, 2287-2295.

20. Eckstein, F., Cassel, D., Levkovitz, H., Lowe, M. and Selinger, Z. (1979) J. Biol. Chem. 254, 9829-9834.

21. Downs, R. W., Jr., Spiegel, A. M., Singer, M., Reen, S. and Aurbach, G. D. (1980) J. Biol. Chem. 255, 949-954.

22. Sternweiss, P. C., Northup, J. K., Smigel, M. D. and Gilman, A. G. (1981) J. Biol. Chem. 256, 11517-11526.

23. Sitaramayya, A., Virmaux, N. and Mandel, P. (1977) Exp. Eye Res. 25, 163-169.

24. Schwabe, U., Puchstein, C. Hannemann, H. and Sochtig, E. (1979) Nature 277, 143-145.

25. Richards, J. M. and Swislocki, N. I. (1979) J. Biol. Chem. 254, 6857-6860.

26. Richards, J. M. and Swislocki, N. I. (1981) Biochim. Biophys. Acta 678, 180-186.

27. Macara, I. G. (1980) Trends in Biochemical Science 5, 92-94.

28. Pope, M. T., Still, E. R. and Williams, R. J. P. (1980) in Molybdenum and Molybdenum-containing Enzymes (Coughlan, M. P., ed.) pp. 1-40, Pergamon, Oxford.

29. Cantley, L. C., Jr., Cantley, L. G. and Josephson, L. (1978) J. Biol. Chem. 253, 7361-7368.

30. Sternweis, P. C. and Gilman, A. G. (1982) Proc. Natl. Acad. Sci. U.S.A. 79, 4888-4891.

31. Mansour, J. M., Ehrlich, A. and Mansour, T. E. (1983) Biochem. Biophys. Res. Commun. 112, 911-918.

32. A. Lewis, H. Zwick, S.T. Schuschereba and A. Hochberg, Biochem Biophys. Res. Communic. (in press).

33. A.R. Spurr, Scanning 3, 97 (1980).

34. J.T. Brenna and G.H. Morrison in Microbeam Analysis eds. A.A. Romig and J.I. Goldstein, San Francisco Press, Inc. (1984) p. 265.

35. Brown, P. K., Gibbons, I. R. and Wald, G. (1963) J. Cell Biol. 19, 79-106.

36. Cohen, A. I. (1969) in The Retina:Morphology, Function, and Clinical Characteristics (Straatsma, B. R., Hall, M. O., Allen, R. A. and Crescitelli, F., eds.) pp. 31-62, Univ. of California, Berkeley and Los Angeles, 1969.

37. Cohen, A. I. (1961) Exp. Eye Res. 1, 128-136.

38. Burnside, B., Smith, B., Nagata, M. and Porello, K. (1982) J. Cell Biol. 92, 199-206.

39. O'Connor, P. and Burnside, B. (1982) J. Cell Biol. 95, 445-452.

40. Burnside, B. (1978) J. Cell Biol. 78, 227-246.

41 O'Connor, P. and Burnside, B. (1982) J. Cell Biol. 95, 445-452.

42. Porrello, K., Cande, W. Z. and Burnside, B. (1983) J. Cell Biol. 96, 449-454.

43. Cohen, A. I. (1965) Anat. Rec. 152, 63-80.

44. Chaitin, M. H., Schneider, B. G., Hall, M. O. and Papermaster, D. (1983) Inv. Ophth. Vis. Sci. (Supplement), 287.

45. Pesacreta, T., Carley, W. F., Webb, W. W. and Parthasarathy, M. V. (1982) Proc. Natl. Acad. Sci. U.S.A. 79, 2898-2901.

46. Barak, L. S., Nothnagel, E., DeMarco, E. F. and Webb, W. W. (1981) Proc. Natl. Acad. Sci. U.S.A. 78, 3034-3038.

47. Barak, L. S., Yocum, R. R. and Webb, W. W. (1981) J. Cell Biol. 89, 368-372.

48. Barak, L. S., Yocum, R. R., Nothnagel, E. and Webb, W. W. (1980) Proc. Natl. Acad. Sci. U.S.A. 77, 980-984.

49. Wong, A. J., Pollard, T. D. and Herman, I. M. (1983) Science 219, 867-869.

50. Usukura, J. and Yamada, E. (1981) Biomedical Res. 2, 177-193.

51. Roof, D. J. and Heuser, J. E. (1982) J. Cell Biol. 95, 487-500.

52. Hagins, W. A. and Jennings, W. H. (1959) Discussion Faraday Soc. 27, 180-190.

53. Borwein, B. (1983) Anat. Rec. 205, 363-373.

54. Yoshikami, S., Robinson, W. E. and Hagins, W. A. (1974) Science 185, 1176-1179.

55. Hagins, W. A. and Ruppel, H. (1971) Fed. Proc. 30, 64-68.

56. Korenbrot, J. I., Brown, D. T. and Cone, R. A. (1973) J. Cell Biol. 56, 389-398.

57. Del Priore, L. and Lewis, A. (1983) manuscript in preparation.

58. J.M. Enoch, Ivestigative Opthalmology 2, 16 (1963).

59. A. Lewis and L. del Proie, Science 60 (accepted).

60. I. Tasaki and T. Nakaye, Science (accepted).

END
DATE
FILMED
3-1988
DTIC